ASTROGEOLOGIC STUDIES

ANNUAL PROGRESS REPORT R-66

July 1, 1965 to July 1, 1966

PART D
SPACE FLIGHT INVESTIGATIONS

DEPARTMENT OF THE INTERIOR

UNITED STATES GEOLOGICAL SURVEY

ASTROGEOLOGIC STUDIES

ANNUAL PROGRESS REPORT

July 1, 1965 to

July 1, 1966

PART D: SPACE FLIGHT INVESTIGATIONS

December 1966

This report concerns work done on behalf of the National Aeronautics and Space Administration

DEPARTMENT OF THE INTERIOR
UNITED STATES /GEOLOGICAL SURVEY

CONTENTS

PART D--SPACE FLIGHT INVESTIGATIONS

INTRODUCTION

This Annual Report is the seventh of a series describing the results of research conducted by the U.S. Geological Survey on behalf of the National Aeronautics and Space Administration. The report is in four volumes corresponding to four main areas of research: Part A, Lunar and Planetary Investigations (with map supplements); Part B, Crater Investigations; Part C, Cosmic Chemistry and Petrology; and Part D, Space Flight Investigations (with a map supplement). An additional volume presents abstracts of the papers in Parts A, B, C, and D.

The long-range objectives of the astrogeologic studies program are to determine and map the stratigraphy and structure of the Moon's crust, to work out from these the sequence of events that led to the present condition of the Moon's surface, and to determine the processes by which these events took place. Work that leads toward these objectives includes a program of lunar geologic mapping; studies on the discrimination of geologic materials on the lunar surface by their photometric, polarimetric, and infrared properties; field studies of structures of impact, explosive, and volcanic origin; laboratory studies on the behavior of rocks and minerals subjected to shock; and study of the chemical, petrographic and physical properties of materials of possible lunar origin and the development of special techniques for their analysis.

Part D, Space Flight Investigations, includes reports on geologic analysis and mapping from Ranger photographs, research on methods of Ranger photogrammetry, an analysis of small lunar craters by comparison with experimentally produced impact and explosion craters, and a sample of the preflight geologic reports prepared for the sites photographed by Lunar Orbiter I.

PROGRESS IN GEOLOGIC TERRAIN MAPPING FROM RANGER PHOTOGRAPHS

By N. J. Trask

INTRODUCTION

Three preliminary geologic terrain maps constructed from the Ranger photographs are included in the map supplement to this report. In this program of Ranger geologic mapping we have attempted to divide the surface materials of the Moon into meaningful units at scales larger than the 1:1,000,000 employed for Earth-based lunar mapping. If such units can be extended over large areas of the Moon by further mapping, they will provide information on the nature and extent of materials to be sampled during the first manned landings as well as a background against which to plan the operations of future missions. Because the Ranger pictures consist of a series in which the scale changes gradually, they have aided in the early study of medium- and high-resolution photographs transmitted by the Unmanned Lunar Orbiter.

The mapping accomplished to date has shown that geologic and physiographic units can be delineated at the larger scales. The problems of mapping the Moon at scales larger than 1:1,000,000 vary with location on the Moon and with scales; the authors of the enclosed maps have necessarily used criteria for the recognition of units which differ from map to map. These preliminary studies together with work on the Lunar Orbiter photographs should, however, eventually result in a generally acceptable set of procedures for mapping the Moon at intermediate and large scales.

PREVIOUS WORK

The main previous analyses and interpretations of the Ranger photographs have appeared in Technical Reports 32-700 and 32-800 of

the Jet Propulsion Laboratory, Pasadena, Calif.; these include contributions by the experimenters on the project as well as short papers by co-workers of the experimenters. Emphasis in these reports has been on considerations of the origins of the several types of features shown on the photographs; several of the reports placed considerable emphasis on terrestrial analogs. In the report covering the Ranger VIII and IX photographs, five preliminary geologic maps of selected areas were included (Carr, 1966; Milton and Wilhelms, 1966; McCauley, 1966; Trask, 1966b; and Schmitt, 1966; all in Shoemaker and others, 1966). These maps provided the starting point for the present program of Ranger geologic mapping.

METHODS OF STUDY

Stereoscopic and monoscopic examination of good quality sets of the Ranger photographs has been the principal method of study used to construct the maps. The base height ratio in pairs of the photographs is very weak for good stereoscopsis; nevertheless, stereoscopic viewing is extremely helpful in emphasizing subtle detail and suppressing the effect of lines and spots due to noise in the receiving system. Only photographs taken near the end of each mission were processed by a computer to remove the effects of scan lines and noise, and these could not be used to make the maps because of scale differences.

The study was begun with the idea that much topographic information could be obtained by the standard methods of photogrammetry and the newer methods of photoclinometry (Watson, 1966). Accordingly, effort was made to apply photogrammetry to the photographs. Photoclinometry, however, proved extremely difficult to apply to the Ranger photographs; for the most part, information derived by this method was not used in the mapping.

Using photogrammetric methods, several reasonably consistent stereo models were obtained, and small topographic maps were produced, the accuracy of which is at present unknown, of course. The photogrammetric information was used to help characterize some of the units defined on the maps. Viewing of the stereo models produced

by the various plotting instruments was also helpful in determining the geology.

Additional information--relative albedo of the lunar surface materials--was obtained for the small-scale and some intermediate-scale maps from full-Moon photographs.

GEOLOGIC BACKGROUND

Geologic maps at a scale of 1:1,000,000 prepared from Earth-based observations provide the background against which to consider the new information that the Ranger photographs have conveyed concerning the lunar surface. An up-to-date review of this work is given by Wilhelms in Part A of this annual report. All the Ranger impact areas were in plains-forming materials--Rangers VII and VIII in plains-forming material of relatively low albedo in the lunar maria and Ranger IX in plains-forming material of intermediate albedo in the lunar terrae. Since these materials will most likely predominate at the site of early manned landings, the detailed geology of these units is of considerable interest. In addition, all three Ranger missions provided a clearer picture of details in the gently rolling to rugged hills and valleys of the lunar terrae.

The Ranger photographs revealed a hitherto unsuspected abundance of craters on the plains-forming materials of both mare and terra and also presence of many very shallow low-rimmed or rimless craters. Interpretations of these features is evidently critical to an understanding of 1) the origin of the present physiography of the plains-forming materials, as well as 2) the origin of the fine-scale texture and structure of the surface of the plains-forming materials. Two principal theories have been advanced. Shoemaker (1965) suggested that most of the craters in the Ranger VII site were of impact origin and that the craters with subdued form were worn-down, eroded features that had once been sharp craters. In a later report summarizing the Ranger VIII and IX results (Shoemaker and others, 1966), he suggested that many craters in the plains-forming materials might be of internal origin; he maintained, however,

that subdued and rounded crater forms were due in large part to ballistic erosion. If ballistic erosion is important in wearing down the fresh form of initially sharp craters, it should produce a surface layer of erosional debris. The existence of such a layer, largely cohesionless or of very low cohesion, is suggested by the morphology of the small craters photographed by Ranger IX (25 m diameter) (Moore, in Shoemaker and others, 1966) and by the pictures returned by the Surveyor I spacecraft (Jaffe and others, 1966). A contrasting model of the surface and of the mode of development of the subdued craters has been suggested by Kuiper (1965) and Kuiper and others (1966), who argue that the subdued craters are primarily collapse features in basalt flows and that the subdued form is a primary attribute. In this model, the original surface of the plains-forming material either is exposed or has been only slightly modified by micrometeorite impact and sputtering; fragmental material would be thin and discontinuous.

In constructing geologic maps from the Ranger photographs, we have attempted to delineate units objectively; assumptions about the nature of the surface have been avoided. As on Earth-based lunar maps, the map units are of two basic types--crater units and extended units. The crater units are limited to the immediate vicinity of craters; the extended units represent the material or materials surrounding the craters and extend throughout the intercrater areas. The intercrater areas are themselves covered by small craters, so the dividing line between crater units and extended units on the Ranger maps is somewhat arbitrary. In the plains-forming materials, the various extended units are defined mainly on the basis of the areal density and morphology of the small craters on them. Larger craters that interrupt the continuity of the extended units and are clearly not related to the surface texture of the latter are mapped separately. Extended units in the plains-forming materials that are delineated on the basis of the areal density and morphology of craters are not strictly equivalent to the rock-stratigraphic units of terrestrial geology; rather they are more

like physiographic units. In some places in the plains-forming materials, units appear to mantle rather uniformly the subjacent topography; that is, they appear to have a base. Such units may in fact be rock-stratigraphic units on the Moon. Material at the surface of the more rugged terra appears to be largely homogeneous on the Ranger photographs; there are many differences, however, in the size and form of the hills which make up the terra topography. Most units in the terra are therefore physiographic.

The remainder of this report summarizes the results of geologic and physiographic mapping in the areas covered by Rangers VII, VIII, and IX. In addition, a separate section is devoted to a discussion of some of the crater statistics generated from the photographs of all three missions and to a consideration of what these statistics reveal concerning the manner in which the surface has developed.

AREA COVERED BY RANGER VII

In the course of mapping at a scale of 1:500,000, R. E. Eggleton has performed a semiquantitative morphologic analysis of the terrain in the Guericke region surrounding the Ranger VII impact point. Relief features have been classified and individually mapped as positive elements (hills and ridges), negative elements (single craters, composite craters, and irregular depressions), scarps, and intervening plains. Both positive and negative elements have been placed in subclasses according to the steepness of their slopes; plains have been differentiated according to topographic textures composed of features too subtle or too small to map individually. The morphologic data can be used to interpret the pattern of faulting in the premare materials. Knowledge of the deformation pattern has aided in the recognition of old crater.

Eggleton has also found evidence for the sequence of formation of individual craters within a local cluster of craters that seem to be part of the field of secondary impact craters around Bullialdus.

A string of craters within the cluster includes three composite craters each of which is a pair of circular craters resulting from two principal impacts roughly alined along the string. In two pairs, the crater farther from Bullialdus has a sharper crest and steeper slopes than the nearer. This suggests that in each case the farther one was formed later so that its ejecta is superimposed on the nearer.

The Bonpland H region being mapped by T. N. V. Karlstrom at a scale of 1:100,000 lies wholly within the mare material of Mare Cognitum. Mapping of this area has proved especially difficult because of the rather poor quality of the photographs transmitted by Ranger VII, the first successful Ranger spacecraft, and the relatively high Sun angle. Work on this area is still in progress at the time of this report.

AREA COVERED BY RANGER VIII

Map units on the 1:250,000 scale map of the Sabine region by H. G. Wilshire are closely similar to those on the 1:100,000 maps of the Moon (compare Morris and Wilhelms, 1967). The mare is treated as one unit, and the terra is broken down into plains-forming material and more rugged terra of various physiographic types. Two large craters, Sabine and Ritter, occupy a significant part of this small-scale map. According to Wilshire, both are probably of internal rather than impact origin. Hummocky ejecta surrounding the craters appears to partly bury the major graben structures Rimae Hypatia I and II that cut the mare material and is therefore probably younger than the mare surface material. However, there are no secondary craters surrounding the ejecta blanket such as are found around impact craters of the same age and size. In addition, the floors of the two craters are higher and rougher than the floors of typical postmare craters of the same diameter.

The Sabine DM region, which I mapped at a scale of 1:50,000, lies wholly within Mare Tranquillitatis. The plains-forming

material of the mare can be divided here into three units: (1) a ridged unit whose areal density of subdued craters is greater than that of the other units and which also has numerous lineaments, low irregular domes, and irregular depressions; (2) a smooth mostly level unit, with fewer craters than the ridged unit and fewer lineaments than the other two units; and (3) a smooth gently undulating unit that occurs around large irregularly shaped craters and has fewer craters than the ridged unit. The nature and significance of these units are difficult to determine from the Ranger photographs, which cover a very limited area. For example, it is not certain whether the units are composed of different materials or the same materials with different physiographic expressions. The smooth undulating material of the third unit listed above appears fresher and possibly younger than the other two. Limited photogrammetric data indicate that it stands slightly above the surrounding terrain. On the Ranger photographs, this material looks possibly like volcanic ejecta that has issued from the irregularly shaped craters it surrounds and has formed undulating plateaulike areas. Lunar Orbiter II photographs of the same material over a much larger area suggest, however, that the irregular craters may be secondary impact craters formed by fragments from the crater Arago and that the undulating material may be ejecta from the secondaries. This uncertainty emphasizes the need for Lunar Orbiter coverage with moderate resolution over large areas of the Moon.

Contacts between the ridged units and the smooth level unit are parallel in some places to well-developed regional lineaments. This parallelism suggests that the contacts may be lines of mild tectonic activity, that surficial debris was collected on down-dropped blocks to form the smooth level material, and that the debris is correspondingly thinner on the uplifted blocks to form the ridged unit. The evidence for a surficial layer of weakly cohesive to noncohesive fragmental debris has already been cited (p. 4). Recognition of the three mare units does not, however, depend on the interpretations placed on them. Useful information

on their origin may be derived from the patterns they form on maps of larger areas prepared from Lunar Orbiter photographs.

AREA COVERED BY RANGER IX

Photographs returned by Ranger IX show the large crater Alphonsus and its immediate vicinity. Geologic mapping at a scale of 1:250,000 of the crater and its surroundings by M. H. Carr permits a reconstruction of the history of the crater in terms of a local stratigraphic column. Carr interprets Alphonsus as a pre-Imbrian impact crater that has undergone subsequent isostatic readjustment and filling. The rim material of the crater is intensely dissected by Imbrian sculpture. The filling material on the floor is mostly of higher albedo and is more cratered than typical mare material; it consists of both ejecta from nearby craters and volcanic materials derived from vents within the crater. Craters with halos of very low albedo, structurally localized along rilles and resembling terrestrial maars, provide the clearest evidence of volcanism. The rim materials of the dark halo craters clearly fill adjacent depressions. Much of the lighter filling material on the floor can be divided into three units characterized by differences in crater frequency; these may be volcanic units of different ages, the most cratered being the oldest. The southwestern part of the crater floor is shallow so that the older crater floor is not completely covered by filling and is exposed at the surface.

No further division of the plains-forming materials on the floor of Alphonsus is possible at larger scales. The 1:50,000 scale map of the Alphonsus GA region by J. F. McCauley therefore emphasizes a morphologic analysis of crater forms. This work is still in progress.

CRATER STATISTICS

One of the chief results of new data derived from the Ranger photographs was the extension of crater size-frequency curves some three orders of magnitude downward in crater diameter from the 1 km limiting resolution on the best telescopic photographs to near

1 meter resolution on the final Ranger frames. Preliminary studies of the crater distribution dealt mainly with the total crater count (Trask, 1966a); that is, all craters were included in the statistics regardless of crater morphology or supposed origin. Cumulative size-frequency diagrams of total craters for the three missions are given in figure 1. The following aspects of the curves are worthy of note.

1. Curves for the maria (Rangers VII and VIII) show a marked upward break in slope at crater diameters of between 5 and 1 km. The very rapid increase in the number of craters in this interval is also measurable on recent high-resolution terrestrial photographs from the Lick Observatory, which became available at about the same time as the Ranger photographs. The existence of the upward break in slope means that extrapolations of crater counts in the maria from earlier Earth-based observations (McGillem and Miller, 1962) give frequencies of small craters that are much too low.
2. Both curves for the maria undergo a second change in slope and become flatter at crater diameters of between 300 and 600 meters. The overall slope of the curves between diameters of 300 and 1 meter is -2. The resultant frequency of craters at 1 meter is, of course, much lower than would be obtained if the higher slopes above 300 meters diameter were maintained.
3. The crater frequency on the plains-forming material of the floor of Alphonsus is as much as an order of magnitude higher than on the maria at diameters of 1 km; the size-frequency curve, however, maintains a slope of -2 over most of its length and merges with the curve for the mare photographed by Ranger VIII at diameters of 10 meters.

In the interpretation of crater statistics derived from the Ranger photographs, it should be borne in mind that both the Sun angle and the trace of the subspacecraft point on the lunar surface differed appreciably in the three missions. The rather high Sun angle in the Ranger VII mission probably results in failure to

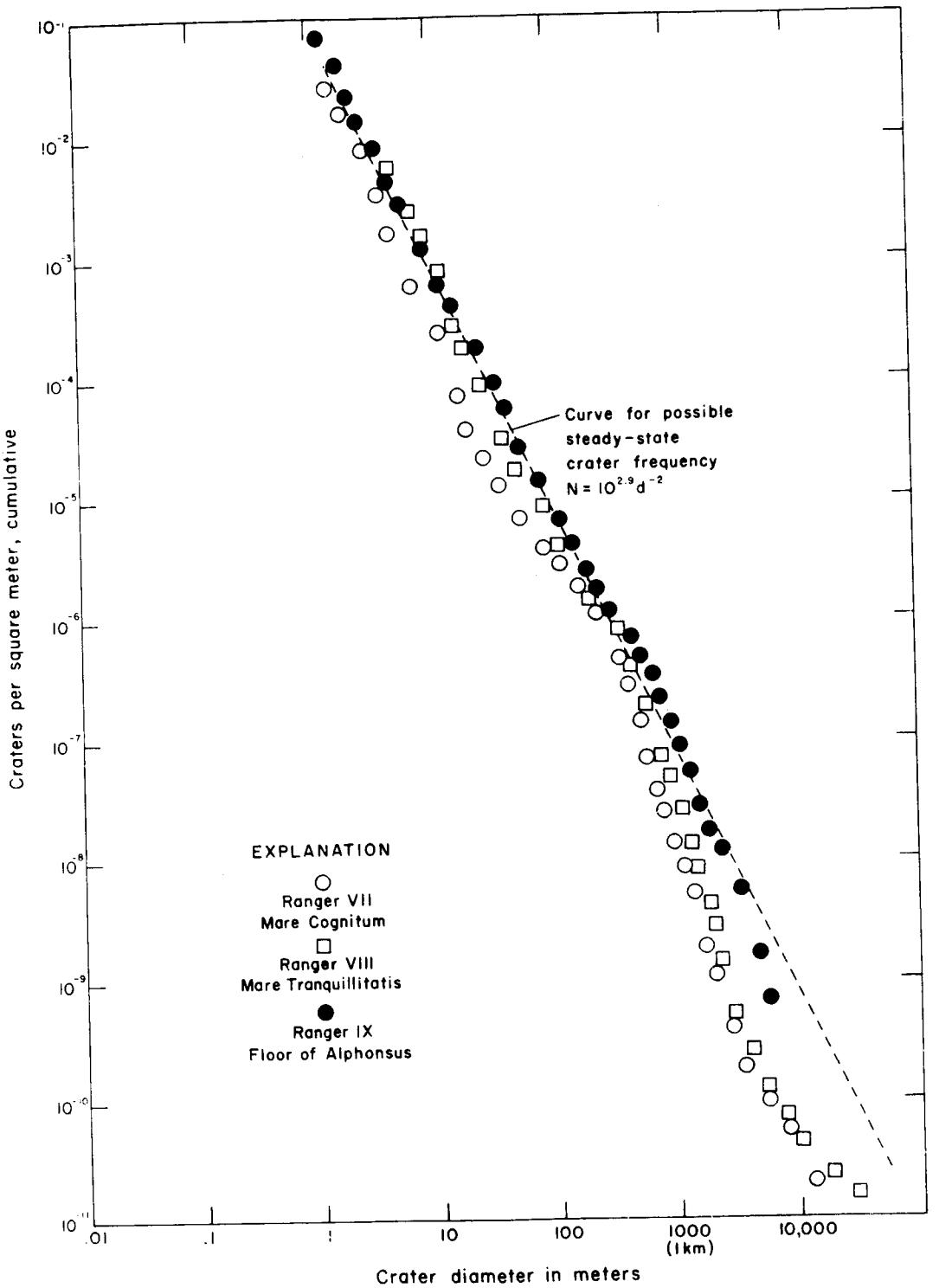

Figure 1.--Comparison of cumulative size-frequency distributions of craters photographed by Rangers VII, VIII, and IX.

detect many subdued craters. In the Ranger VIII mission, the spacecraft was maintained in the cruise mode without terminal maneuver so that successive photographs protray overlapping rather than nested areas; the crater statistics are thus a composite with the statistics for small craters coming from a different area than the statistics for large craters.

The close agreement of the frequencies of small craters on three diverse surfaces sampled by the Ranger spacecraft (fig. 1) indicates that the most recent cratering history on all three has been similar. The high-resolution photographs from Lunar Orbiter give the same impression and have a rather monotonous similarity with a few exceptions. At larger crater diameters (100 m to 1 km), there are much larger differences in the crater frequencies (fig. 1), a situation also evident on Orbiter photographs. Proposed cratering histories of the Moon must account for these fundamental observations.

The observed frequencies of small craters on the three surfaces are much lower than the theoretical expected frequency calculated by assuming a constant flux of objects entering the Earth-Moon system and an appreciable age for the cratered surfaces of 500 million years or more (Shoemaker and others, 1963; Moore, 1964; Shoemaker, 1965). Clearly, if the flux has remained constant, many craters that once existed on these surfaces have been destroyed. In the report on Ranger VII, Shoemaker (1965) proposed that such destruction would take place by the bombardment of primary and secondary objects; secondary fragments moving on low trajectories would be especially efficacious in reducing the height of crater rims and filling in crater floors. Since the formation of new craters results in the destruction of old ones, a steady state condition might develop during which the crater frequency for craters smaller than a given size does not change with time. The close agreement of the frequencies of small craters on all three surfaces sampled by the Rangers led me to suggest that the steady state condition for a level surface on the Moon could be estimated from the combined data of figure 1 (Trask, 1966a). The dashed line

represents a power function toward which the crater size-frequencies appear to be tending. This line also passes through values for the frequencies of very large craters on the Southern Highlands, values which may represent a steady state frequency for very large craters. The changes in slopes on the curves for Rangers VII and VIII between 300 and 600 meters may be taken as the point at which the crater distributions reach a steady state condition for craters smaller than this size. This limiting diameter would increase with time. The distribution on the floor of Alphonsus may be in a steady state at all diameters below 1 km.

Additional information on the cratering history of the Moon may be obtained by adding information on crater morphology to the data on crater size and crater frequency. There is plainly a wide range in the morphology of the craters from very gentle depressions to sharply sculptured forms with steep raised rims; also, there is a continuum of types between these two extremes. The final frames of all three Ranger missions show an increase in the proportion of sharp craters (fig. 2) (Trask, 1967). The increase is also evident on high-resolution Orbiter photographs, and its explanation may eventually provide an added constraint on possible cratering histories of the Moon.

Several explanations for the increase in the proportion of sharp craters between 30 and 10 meters can be suggested at present. Le Poole (in Kuiper and others, 1966) identified the sharp craters with primary impact craters and the gentle depressions with collapse features; he correlated the rapid increase in the proportion of sharp craters with an upward break in the present observed flux of meteorites as published by Hawkins (1964). The measured frequency of the small craters which Le Poole classifies as primary requires that the magnitude of the flux gradually increase from zero to its present level over geologic time. This interpretation rules out any significant destruction of craters since the plains-forming materials were evolved; but the continuum of crater types from sharpest to most subdued suggests that crater destruction in some form has played a major role in the evolution of these surfaces.

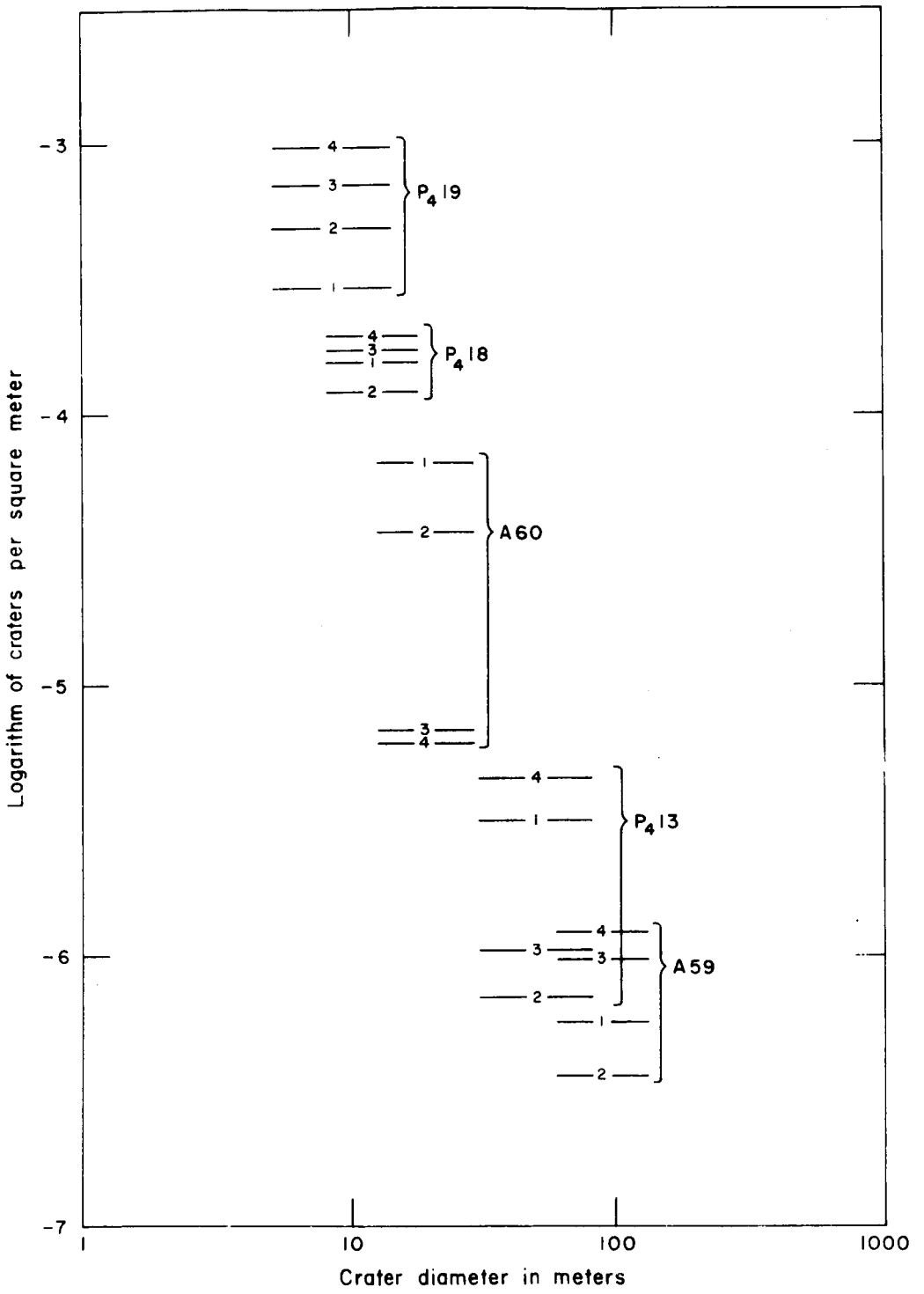

Figure 2.--Size-frequency distributions of different types of craters in the Ranger VIII impact area. Type 1 craters sharpest, type 4 most subdued.

In a simple steady state condition of crater formation and destruction, the rate of crater formation is a simple power function of crater diameter, and the rate of crater destruction is proportional to the rate of crater formation (Moore, 1964). In such a model, the proportion of sharp craters should be the same at all crater diameters because the rate of destruction would be the same for all crater diameters. The fact that the proportion of sharp craters is not constant with crater diameter but varies in a regular way (fig. 2) indicates that the cratering history of the Moon has departed from a simple steady state development. The rate of crater formation or the rate of crater destruction or both may have departed from a simple power dependence on crater diameter. Periodic volcanic outpourings are a mechanism of crater modification which when added to ballistic erosion by younger craters would result in variations in the proportion of sharp craters. The degree to which craters are obliterated or softened would depend on the thickness of the flow. O'Keefe (1966) has consistently proposed such a process.

Crater destruction by episodic mass movement is another mechanism that could result in the present distribution of crater morphologies while the rate of crater production remained essentially constant. Craters larger than approximately 100 meters in diameter would be more apt to have been subdued by mass movement because they are generally older than the smaller craters and would have undergone seismic shaking more often.

I find appealing a history in which the rate of crater formation, and the attendant rate of crater destruction due to interaction of craters, has varied over geologic time. The lunar surface would have been intensely bombarded by fragments of all sizes during the final stages of its accretion; this would have been followed by a lengthy period of "sandblasting" by very small particles but without the formation of large craters; finally, the flux of impacting objects would have gradually increased by collisions and grinding in the asteroidal belt in the manner

proposed by Anders (1965). Subdued craters 100 meters in diameter and larger would be very old craters that have undergone lengthy bombardment by dust-size particles; the generally sharper smaller craters would result from more recent impacts by fragments from the asteriodal belt. Such a cratering history is similar to that proposed by Kuiper and others (1966); however, in my model the large subdued craters are mostly impact craters, many probably secondary impact craters, rather than passive collapse depressions; and fragmental debris covers the surface.

Crater statistics from Lunar Orbiter photographs, especially when combined with statistics on very small craters from Surveyors, may make it possible to choose between these alternatives.

SUMMARY

Analysis of the more than 17,000 photographs transmitted by the three successful Ranger spacecraft has shown that at large scales, the surface materials can be divided into units with differing characteristics. The plains-forming materials in particular exhibit rather sharp contacts between units with contrasting frequencies of craters and small differences in surface texture. The engineering properties of these several units could conceivable be different, so their accurate mapping by Lunar Orbiter and other remote sensing instruments is essential.

Data on the size-frequency distributions of craters, for both total craters and for the total broken down into morphologic classes, constitute the most exact and reproducible information derived from the photographs. However, these data alone do not provide a unique answer to the problem of reconstructing the cratering history of the Moon. The crater morphologies together with the nature of the surface as seen by Surveyor I strongly suggest that destruction of craters smaller than 1 km diameter has played in important role in that history. The morphologies also indicate that the history has departed in some way, perhaps only slightly, from a simple steady state development in which a constant flux has destroyed old craters at the same rate as craters are formed.

REFERENCES

Anders, Edward, 1965, Fragmentation history of asteroids: Icarus, v. 4, no. 4, p. 399-408.

Carr, M. H., 1966, The structure and texture of the floor of Alphonsus, in Ranger VIII and IX, pt. 2, Experimenters' analyses and interpretations: California Inst. Technology, Jet Propulsion Lab. Tech. Rept. 32-800, p. 270-275.

Hawkins, G. S., 1964, Interplanetary debris near the earth, in Annual review of astronomy and astrophysics, v. 2: Palo Alto, Calif., Annual Reviews, Inc., p. 149-164.

Jaffe, L. D., and others, 1966, Surveyor I--Preliminary results: Science, v. 152, no. 3730, p. 1737-1750.

Kuiper, G. P., 1965, Interpretation of Ranger VII records, in Ranger VII, pt. 2, Experimenters' analyses and interpretations: California Inst. Technology, Jet Propulsion Lab. Tech. Rept. 32-700, p. 9-73.

Kuiper, G. P., Strom, R. G., and Le Poole, R. S., 1966, Interpretation of the Ranger records, in Ranger VIII and IX, pt. 2: California Inst. Technology, Jet Propulsion Lab. Tech. Rept. 32-800, p. 35-248.

McCauley, J. F., 1966, Intermediate-scale geologic map of a part of the floor of Alphonsus, in Ranger VIII and IX, pt. 2: California Inst. Technology, Jet Propulsion Lab. Tech. Rept. 32-800, p. 313-319.

McGillem, C. D., and Miller, B. D., 1962, Lunar surface roughness from crater statistics: Jour. Geophys. Research, v. 67, no. 12, p. 4787-4794; discussion by J. W. Salisbury, v. 68, no. 7, p. 2065; reply by author, p. 2066.

Milton, D. J., and Wilhelms, D. E., 1966, Geology from a relatively distant Ranger VIII photograph, in Ranger VIII and IX, pt. 2: California Inst. Technology, Jet Propulsion Lab. Tech. Rept. 32-800, p. 302-313.

Moore, H. J., 1964, Density of small craters on the lunar surface, in Astrogeol. Studies Ann. Prog. Rept., August 1962-July 1963, pt. D: U.S. Geol. Survey open-file report, p. 34-51.

Morris, E. C., and Wilhelms, D. E., 1967, Geologic map of the Julius Caesar region of the Moon: U.S. Geol. Survey Misc. Geol. Inv. Map I-510 (in press).

O'Keefe, J. A., 1966, Lunar ash flows, in Hess, W. N., Menzel, D. H., and O'Keefe, J. A., eds., The nature of the lunar surface: Baltimore, Johns Hopkins Press, p. 259-266.

Schmitt, H. H., 1966, Utilization of high-resolution photographs in manned lunar geologic investigations, in Ranger VIII and IX, pt. 2: California Inst. Technology, Jet Propulsion Lab. Tech. Rept. 32-800, p. 326-335.

Shoemaker, E. M., 1965, Preliminary analysis of the fine structure of the lunar surface, in Ranger VII, pt. 2: California Inst. Technology, Jet Propulsion Lab. Tech. Rept. 32-700, p. 75-134.

Shoemaker, E. M., Hackman, R. J., and Eggleton, R. E., 1963, Interplanetary correlation of geologic time, in Advances in the astronautical sciences, v. 8: New York, Plenum Press, p. 70-89.

Shoemaker, E. M., and others, 1966, Progress in the analysis of the fine structure and geology of the lunar surface from the Ranger VIII and IX photographs, in Ranger VIII and IX, pt. 2: California Inst. Technology, Jet Propulsion Lab. Tech. Rept. 32-800, p. 249-337.

Trask, N. J., 1966a, Size and spatial distribution of craters estimated from the Ranger photographs, in Ranger VIII and IX, pt. 2: California Inst. Technology, Jet Propulsion Lab. Tech. Rept. 32-800, p. 252-263.

_____1966b, Preliminary geologic map of a small area in Mare Tranquillitatis, in Ranger VIII and IX, pt. 2: California Inst. Technology, Jet Propulsion Lab. Tech. Rept. 32-800, p. 319-326.

Trask, N. J., 1967, Distribution of lunar craters according to morphology from Ranger VIII and IX photographs: Icarus, v. 6, no. 2, p. 270-276.

Watson, Kenneth, 1966, Photoclinometry from spacecraft images, in Lunar orbiter--Image analysis studies report, May 1, 1965 to January 31, 1966: U.S. Geol. Survey open-file report, p. 1-21.

RANGER PHOTOGRAMMETRY

By J. D. Alderman and S. C. Wu

INTRODUCTION

Ranger missions VII, VIII and IX were successful in their primary objective: to obtain closeup photographs of the Moon that would provide information about small lunar topographic features. This pioneering effort was analogous to Amie Laussedat's balloon photography in 1858 and, in the photogrammetric sense, comparable in quality; the basic difference is that Laussedat's photographic coverage was superior in terms of geometry for use in stereoplotting instruments.

The photogrammetric aspects of Ranger vidicon imagery were discussed in a report by Heacock and others (1966). The instrumentation objectives of the Ranger photogrammetric research program were: (A) To develop a stereo anaglyphic projection plotting system to accommodate (1) extreme and variable camera axis tilts; (2) large camera range differences; (3) base to height ratios down to 0.1. (B) To develop a technique for generation of stereo models having a relative and assumed absolute orientation in an analytical stereo plotter. One result of the achievement of these objectives would be to provide the geologist with a stereo model of such quality that relative height measurements over any quarter section of the neat model could be determined to an accuracy of 10 percent (e.g., the slope of a crater wall determined by model height of perspective center (Bz) differences of two or more selected points would be within 10 percent of the true slope). Another result would be that with the stereo model, relief characteristics and their spatial relationship could be reliably estimated. A secondary goal was to produce reiterative form-line maps of the models using varying orientation modes and, if possible, different operators. These maps would serve as bases for geologic mapping and, more important, would provide calibration data for photoclinometric techniques.

The development of a stereo anaglyphic plotting system described below was a design dictated mainly by economic consideration and to a lesser degree by a strict time limitation. In order to experiment with other systems, a limited time was rented on an Analytic Plotter (AP/C) and several models were studied as described below. Although on some models fairly precise relative height measurements could be made in limited areas, no satisfactory form-line maps were produced by either system. If the Ranger imagery, with its unconventional geometry, image smear, low sun angle, etc., had the metric characteristics of a cartographic camera, the photogrammetric effort might have succeeded. Apparently, TV imagery requires extensive calibration and either specialized plotting equipment or complex filtering techniques. One such selective-filtering technique is the laser scan method, which performs a Fourier transform where the high frequencies (mainly noise) can be filtered out. Unfortunately the method does not yet satisfy the requirements of photogrammetry.

MODIFIED ANAGLYPHIC PROJECTION PLOTTING SYSTEMS

Second-order anaglyphic projection systems are designed basically for compilation of conventional photography where overlaps are in the range of 50 to 60 percent, tilts are limited to ± 3° maximum deviation from required pointing of the optic axis, and the perspective point is at a constant height. The systems are intentionally limited in tilt accommodations, the maximum being $22\frac{1}{2}°$ for conventional convergent photography. The physical size of projectors, dictated by either a lens condensing system (Zeiss) or an elipsoidal reflecting unit (Balspex or ER55), is the major limiting factor of base-to-height ratio accommodation, the limit being approximately 0.4. The lens and principal distance of most systems are set and allow for little flexibility of the normal projection distance, hence placing a limitation on the allowable height of perspective center (Bz) difference between two projectors. The projector support bar is rigid, and only the Z motion of the projector will give a Bz difference.

With the above limitations, anaglyphic projectors were modified so as to increase these latitudes. To add even more versatility, three projector types (two distinct systems) (figs. 1-4) were adapted to handle unconventional Ranger stereo imagery, and a ratio printer (fig. 5) was designed and produced which would provide diapositives at the correct scales.

MODEL SETUP PROCEDURE

Relative orientation of models of Ranger photographs departs radically from conventional procedures in the sense that known and assumed parameters are set prior to the final parallax adjustment. After interior orientation is achieved by centering the diapositive plate to the plate holder with the reference of the center reticle, both projectors are positioned within a calculated or desired base separation by means of plumb lines. They are then leveled, and their height (Bz) above a table (fig. 3) that serves as the common reference datum is set by means of a micrometer rod. The height at which each projector is set is determined by the tilt angle and the range listed in JPL trajectory data.

ω and φ are unknown parameters in the Ranger camera pointing. The system used in this procedure is to orient each projector so that the principal line of the plate is parallel to the projector's X axis. Thus each projector can be entirely rotated about its Y axis (through φ angle) and the angle ω remains zero. The reticles including principal points and nadir points of the pair of overlapped photographs in the model are plotted on stable base material at model scale in the local selenodetic coordinate system in which the X-axis pierces the principal point of each photograph. This system makes the datum of the model parallel to the Y-Z plane of this orthogonal coordinate system.

Relative orientation is begun by projecting the center reticle of the upper projector so that it is coincident with its nadir point plotted on the mylar sheet. The sheet is then rotated about the nadir point in a way that allows the center reticle of the

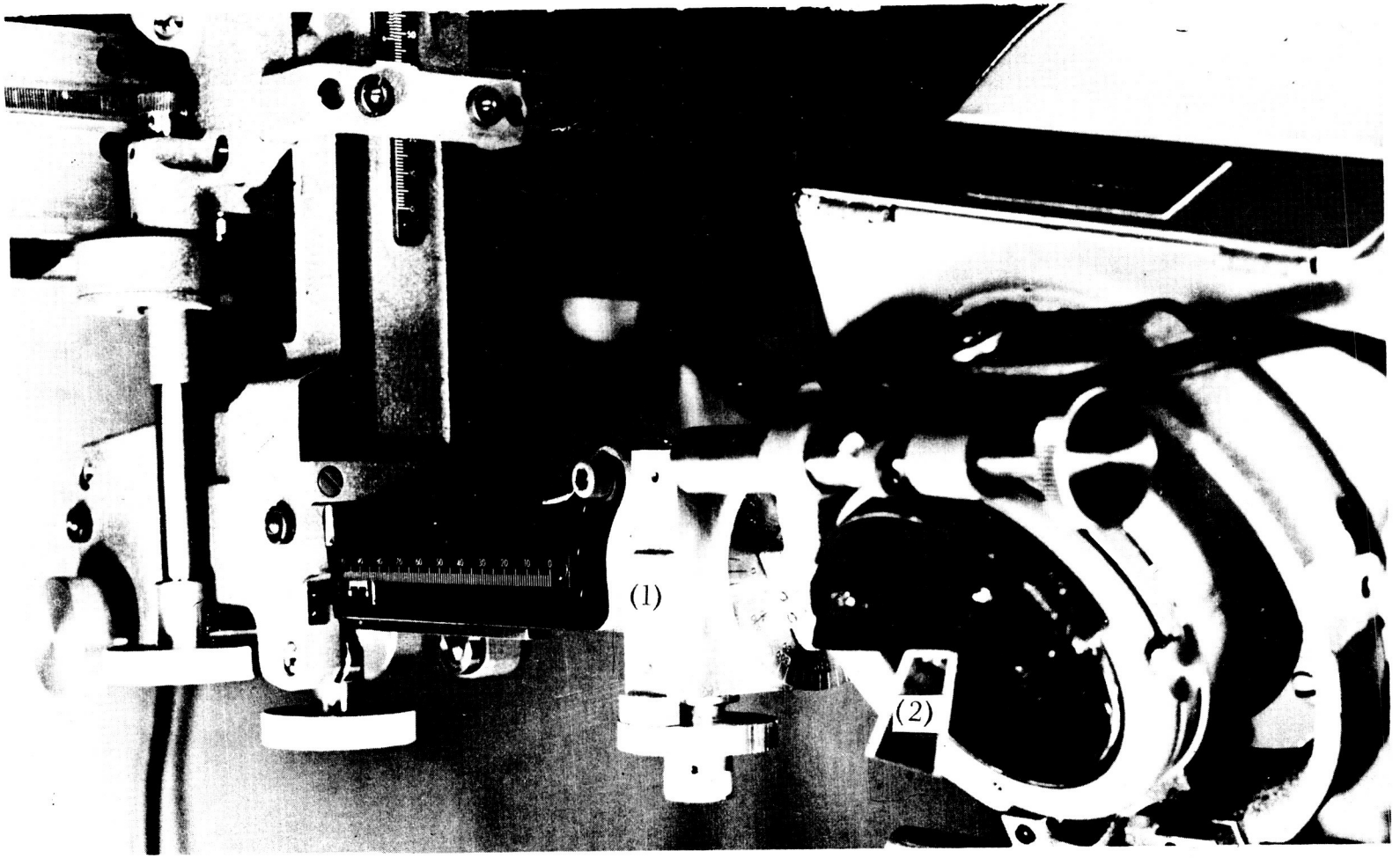

Figure 1.--Modified ER55 projector. (1) Gear box for Y motion and (2) mirror for image displacement.

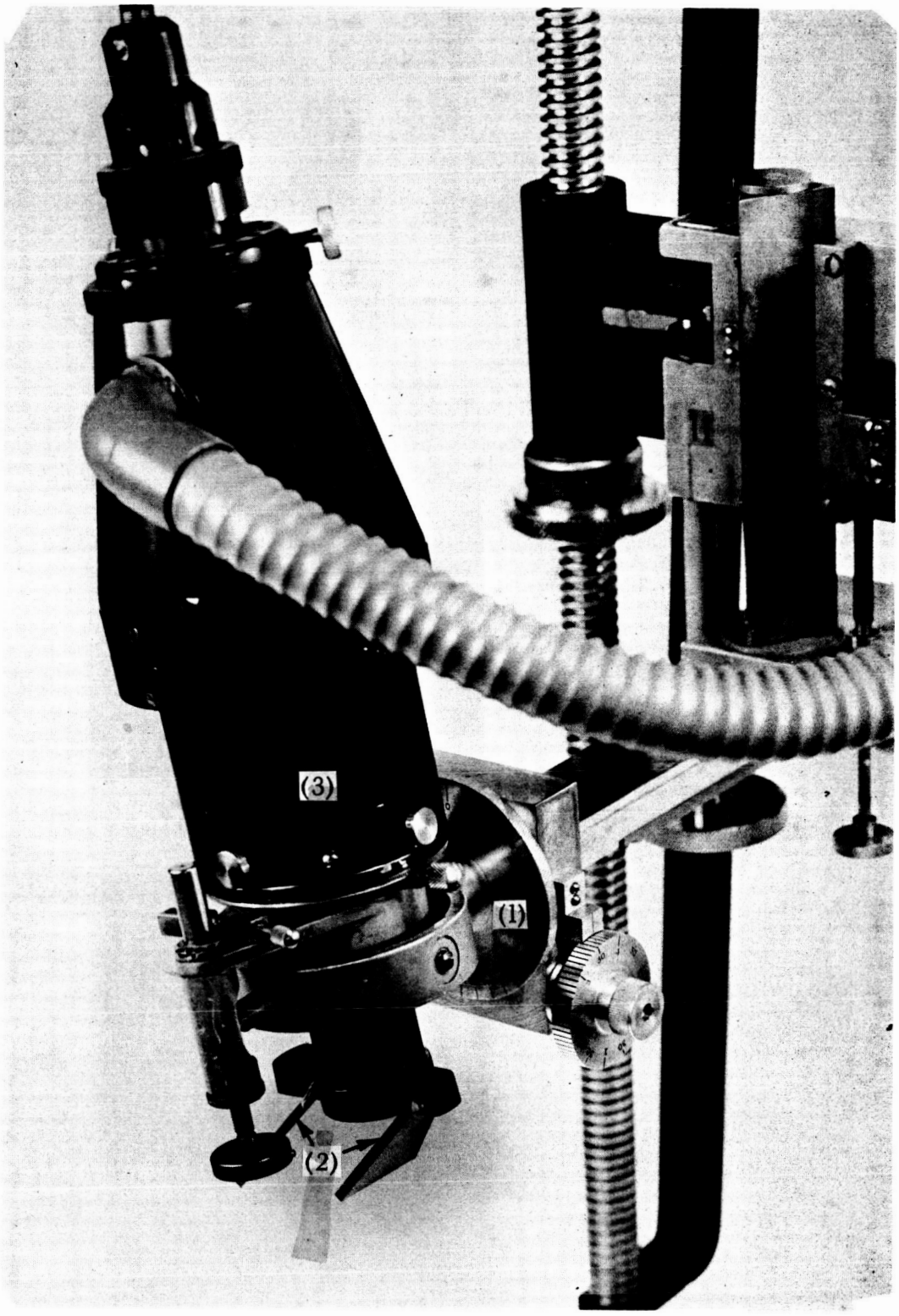

Figure 2.--Modified Zeiss projector. (1) Gear box, (2) double mirror, and (3) machined housing.

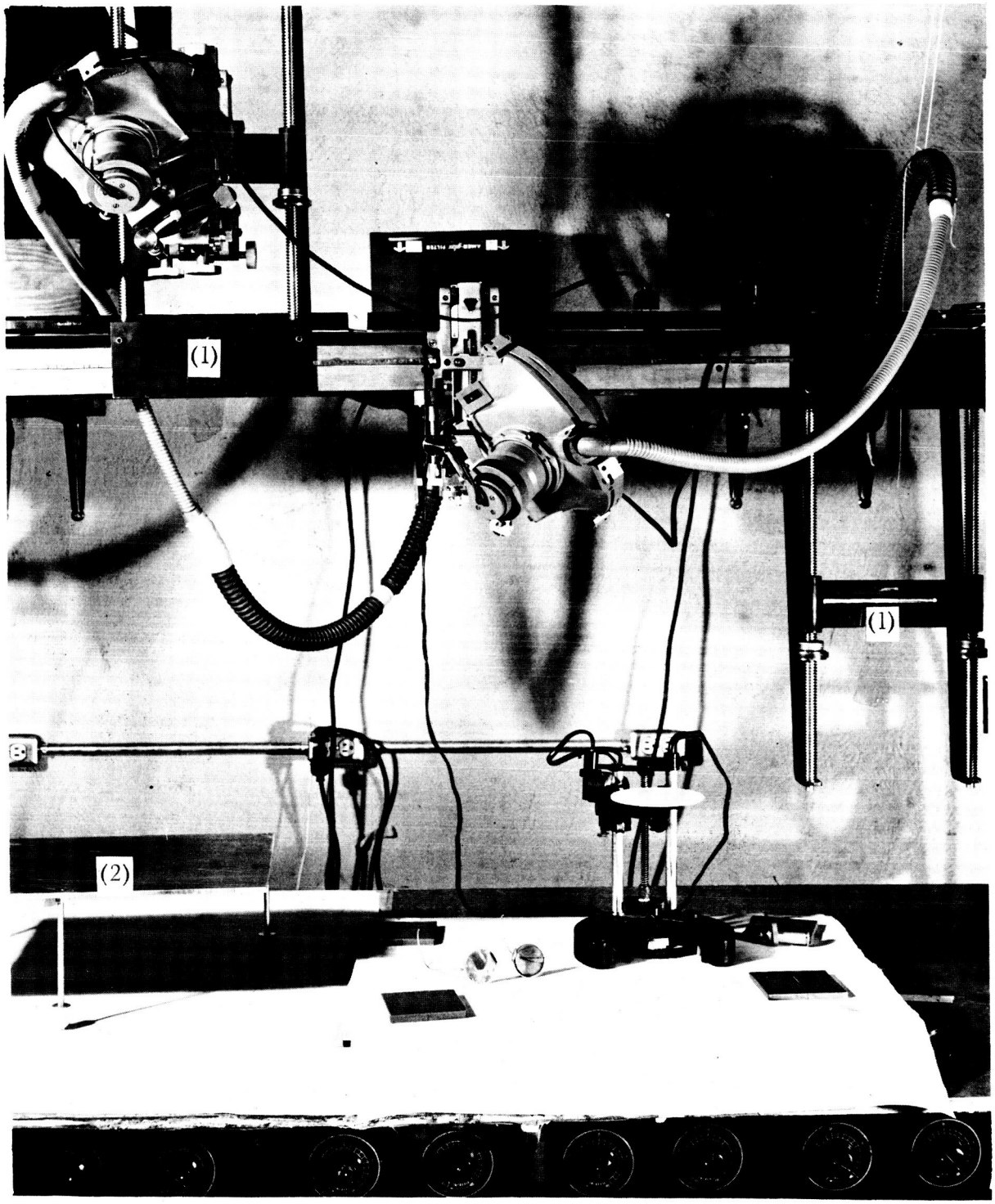

Figure 3.--ER55 model setup on supporting rig (1). (2) Adjustable table for datum reference.

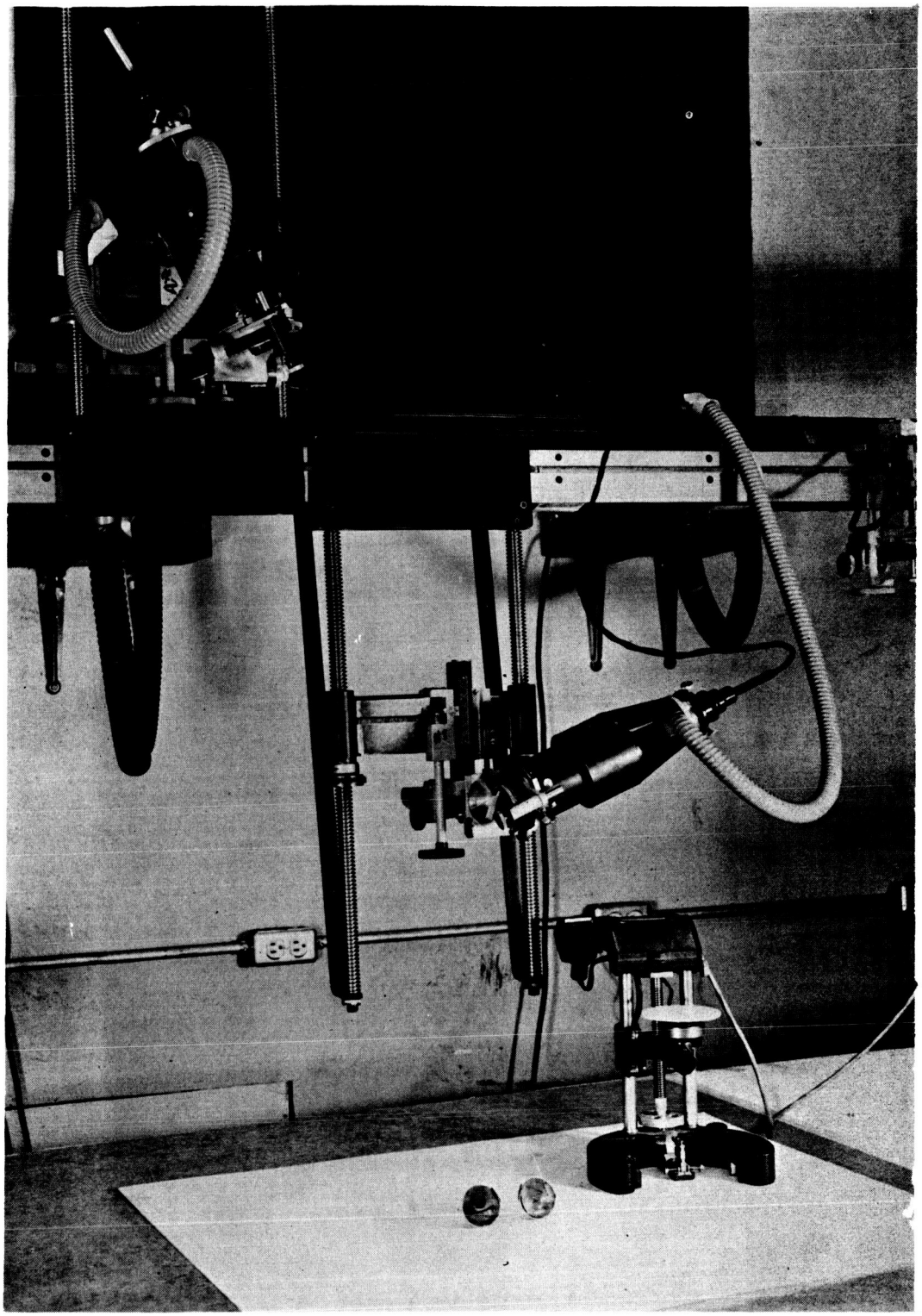

Figure 4.--Zeiss model setup on supporting rig.

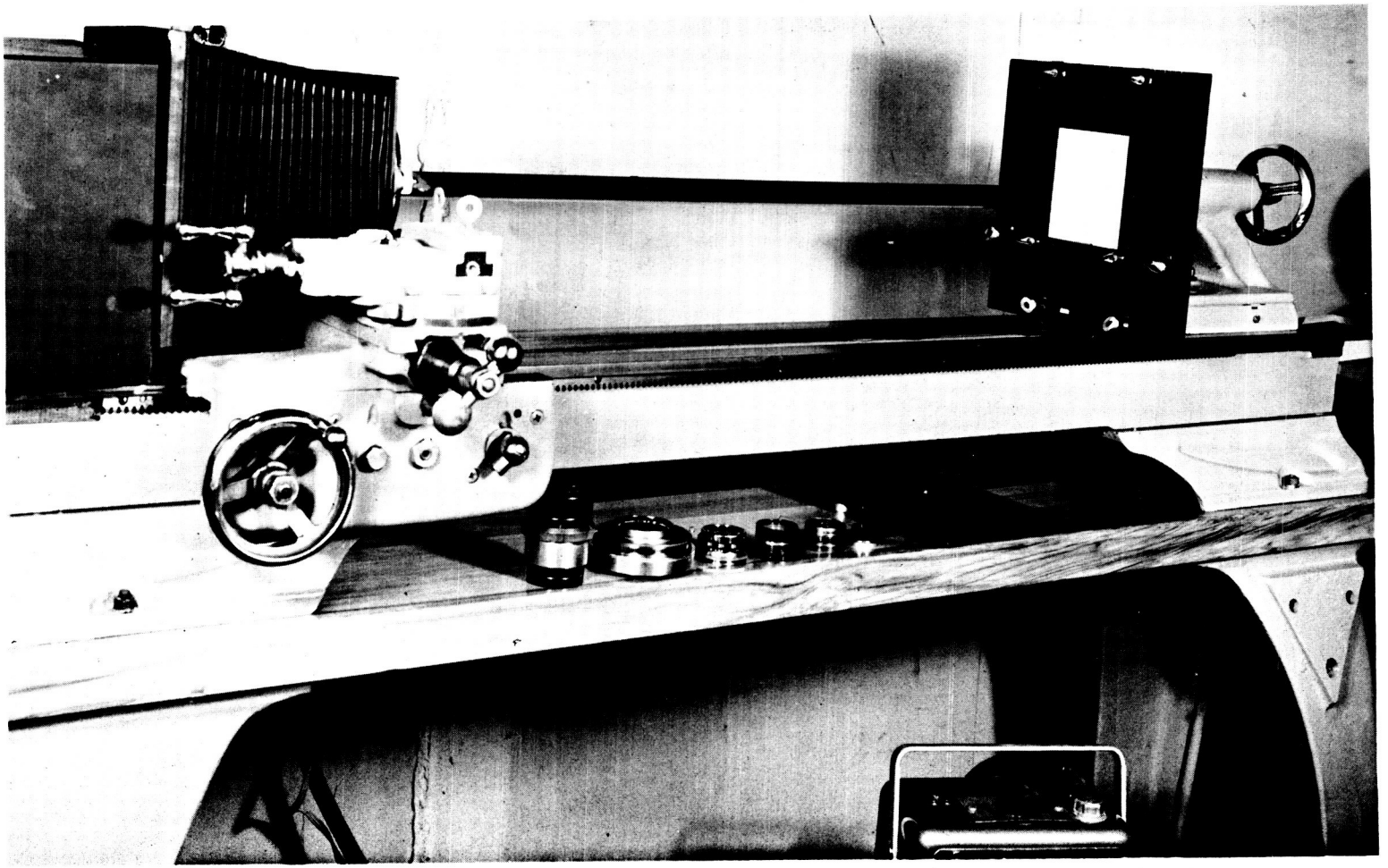

Figure 5.--Ratio printer on lathe bed.

projector to move along the principal line when the tilt angle φ is introduced. Then the mylar is fixed, and the upper projector is rotated through its swing angle until image of reticles is relatively parallel to the plotted reticles.

The lower projector is moved along its various axes until its center reticle is coincident with its equivalent plotted nadir point. It is then tilted downward to the right an amount equal to the complement of its tilt angle. Finally, the projector is rotated as was the upper one to where the image of reticles is parallel to the plotted reticles.

Theoretically, the model should now be oriented relatively parallax free. Unfortunately the projector instability usually introduces appreciable amounts of Y-parallax which are removed by conventional procedures.

The recurring results with this method were as follows:

1. Residual parallax was seldom observable. This was probably the result of very weak geometric stereo; deliberate introduction of large projector tilts produced barely discernible parallaxes.
2. Excessive datum tilts could not be removed by parallax adjustments.
3. What appeared to be exact reproduction of model spatial parameters in independent model setups would produce models with different datum tilts.

ANALYTIC PLOTTER PROJECT

Through the cooperation of Mr. Lloyd Herd of the Ohio State Highway Department, the U.S. Geological Survey was granted a 4-week period to attempt photogrammetric reduction of selected Ranger stereo pairs on the Department's analytic plotters at Columbus, Ohio.

The analytic plotter (AP/C) consists of two high-precision stereocomparators (the viewing units), a digital electronic high-speed computer, and an electronically controlled XY coordinatograph. A basic analytical solution is preprogrammed in order to reconstruct

stereo models based on mathematical formulas. These models enable correction for lens distortion, film shrinkage, curvature, atmospheric refraction, and any known systematic errors. The corrections are entered into the computer as digital values.

Not all combinations of the maximum variables can be displayed on the plotter because its computer is programmed for set ranges of the various quantities. The greatest restriction--the measuring range of Bz--results solely from the physical limit of the plotter motion. For example, the limitation of the interior variable distance is ± 4,180 mm. The computer is programmed for a range of photo-to-model scale of 0.50 to 2.00. For the Ranger models, the three rotation angles are limited. Therefore, the existing AP/C programs were specially modified so that large tilt angles could be processed.

After these modifications were made, the swing angle (k) could be rotated as much as 180°, and the X and Y tilt angles could be rotated ● 90°.

Orientations and Parameters

Operation begins with a pair of photographs for which the orientation elements are not accurately known. First, the two plates are set on the slide carriages. Normally, setting them approximately in the center of each carriage reduces the number of iterations by the computer.

Orientation elements

Before the orientation procedure begins, approximate values for all the elements of interior, relative, and absolute orientation must be prepared for entering. These elements include model scale, focal length, the six parameters Bx, By, Bz, ω, φ, and k as well as the control point data for absolute orientation.

Model scale should be determined considering the limitation of the photo-to-model scale ratio, which is from 0.50 to 2.00. In other words, the restriction for both Bz's should be in the range of 1/2 to 2 of each focal length, respectively.

The quantities Bx, By, and Bz are the coordinates of each camera position with respect to the model center in model scale. The angles k, ω and φ are the swing, X-tilt, and Y-tilt angles of the camera axis with respect to the axes parallel to the model axes. For the model coordinate system, a right-hand orthogonal coordinate system is adopted, and all positive angles are measured counterclockwise when viewed along each axis to the origin, which is the model center.

As an illustration, the model of FA1 and FA2 of Ranger IX was processed on the AP/C. The model scale was chosen as 1:100,000 because the scales and the principal distances of these two diapositives are:

$$S_1 = \frac{1}{95,690} \qquad F_1 = 79.178 \text{ mm}$$

$$S_2 = \frac{1}{96,500} \qquad F_2 = 213.416 \text{ mm}$$

The ratio of photo-to-model is then 1.04, which is in the range of limitation.

The Bz of each photograph can be converted into the model scale from their actual altitude such that,

$$Bz_1 = 7.1956 \text{ km} \times Sm = 71.956 \text{ mm}$$

$$Bz_2 = 19.5729 \text{ km} \times Sm = 195.729 \text{ mm}$$

The determination of Bx and By is somewhat different from conventional photogrammetry because we know only one tilt angle which is a combination of the components ω and φ. The two diapositives are set on the stage plates so that the principal line, which is the line between the nadir and principal point on the plates, is parallel to the plotter X-axis. Thus, when a given tilt angle for the element φ is entered into the computer, ω will be zero.

In the model orientation the principal point of the lower photograph, which is the photograph on the right in the model set-up, was used as the model center. Therefore, elements Bx and By of each plate, with respect to the center of the model, were determined as follows:

Since we know the selenodetic coordinates of the principal points, and the nadir points, as well as each reticle of the two photographs, the distances between PP_1 and NP_1, PP_1 and NP_2 as well as the angle α, which is the difference of aximuth between NP_2 to PP_1 and NP_2 to PP_2, can be calculated from the computed Y Z coordinates (fig. 6) since the ground coordinates can be computed from their longitude and latitude offered by JPL by adopting the local selenodetic coordinate system.

Angle: $\alpha = (NP_2 \longrightarrow PP_2) - (NP_2 \longrightarrow PP_1)$

$= 78°4.06' - 69°28.6'$

$= 8°35.5'$

Distances: PP_1 to NP_1 = 2.4357 km

PP_1 to NP_2 = 8.2065 km

$Bx_1 = PP_1$ to NP_1 = 2.4357 km x Sm

$= 24.357$ mm

$Bx_2 = (PP_1$ to $NP_2)$ cos α = - 8.206 km x cos $8°35.5'$ x Sm

$= - 8.1144$ km x Sm = - 81.144 mm

$By_1 = 0$

$By_2 = (PP_1$ to $NP_2)$ sin α = - 8.2065 km x sin $8°35.5'$ x Sm

$= 1.2260$ km x Sm = - 12.260 mm

And as mentioned before,

$\varphi_1 = t_1 = 18.2481°$ $\omega_1 = 0.0°$

$\varphi_2 = t_2 = 18.1217°$ $\omega_2 = 0.0°$

For k, we assumed that the principal line of each plate is parallel to the machine X-axis, and since the model center is at the center of the FA1 photograph, we set $k_1 = 0$ and the different values of swing angles can be looked up from the JPL data to be the value of k_2 as

$k_1 = 0.0000°$

$k_2 = 98.7290° - 98.7720° = -0.0430°$

Values of all the orientation elements may be entered by the

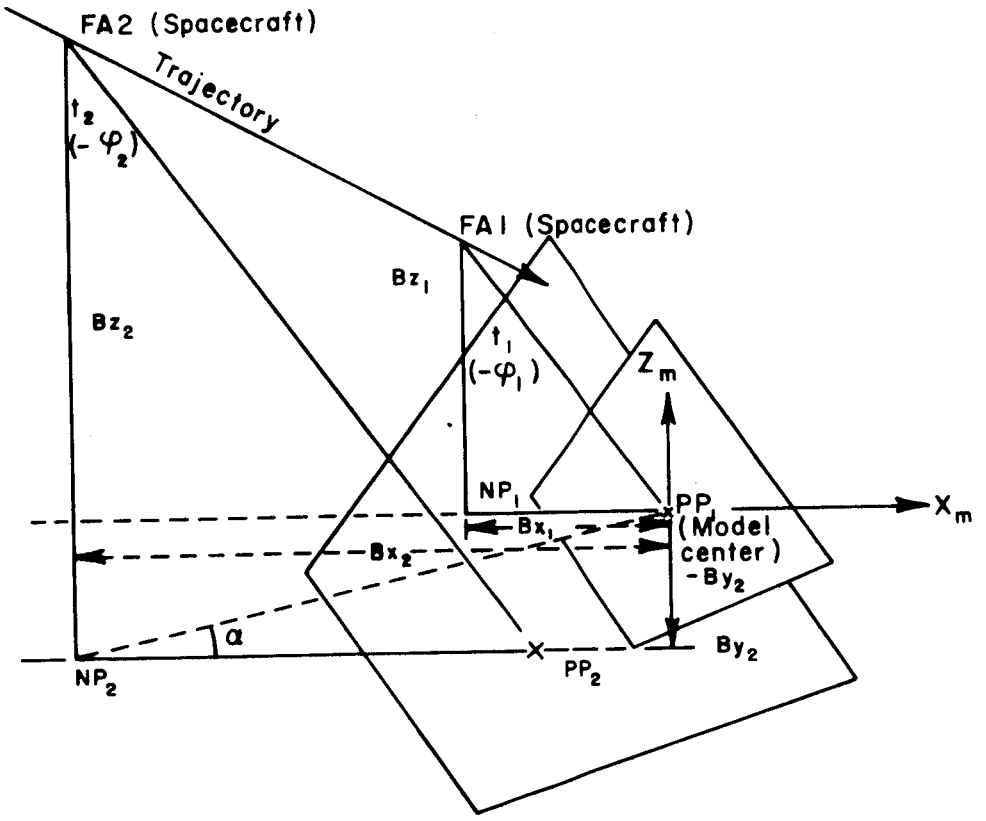

Figure 6.--Geometry of parameters for AP/C.

Operation Orientation Element push buttons whenever they are needed.

Interior orientation

After proper program tapes have been read into the computer, the values of model scale, focal length, and Bz of each photograph are entered. Then the photo coordinates of the four fiducial points on each photograph are measured by setting the floating mark in coincidence with each fiducial mark. At this point the original geometric condition of the two cameras is reconstructed by the calculated perspective center of the camera. Then all photopoint image X and Y coordinates are calculated with respect to the computed center of the camera. Now, the model coordinates X_m, Y_m and Z_m should be set to zero at the center of the right photograph.

For Ranger photographs, any group of four symmetric reticles can be used for this purpose.

Relative orientation

Relative orientation is based on measurements of Y-parallax using from 5 to 12 points in the model. Programs for this purpose solve continuously the set of equations which locate the measured points on each pair of photographs corresponding to a given point in the three dimensional model. Then values of corrections for the approximate orientation elements can be automatically calculated by the computer based on the measured Y-parallaxes.

Therefore, the first step after proper programs have been fed into the computer is to enter initial estimates of orientation elements Bx, By, k, ω, and φ by the Relative Orientation Element push buttons. The Y-parallax of each point in the model is eliminated by the operator by differential displacement using incremental input switches in the Y-position of the two photographs. During this process the amount of motion required is recorded as the Y-parallax of each point and is entered individually by activating the Orientation Step Selection push buttons. Then corrections for orientation elements are calculated and automatically entered into the corresponding orientation elements. The program at this time

automatically retraces the movement of the Y-axis of the photo following the element corrections.

Since this relative orientation procedure is only approximate, it is normally repeated several times before adequate relative orientation is achieved. In general, it is impossible to have zero values for all orientation element corrections. The sum of squares of the corrections is also calculated. This may give the operator a criterion when a certain minimum correction value is approached. In general, sufficiently good relative orientation for compiling is reached when linear corrections are less than 0.1 mm and angular corrections are less than 0.02°.

Absolute orientation

Absolute orientation is performed by entering the coordinates of assumed control points and locating those control points in the stereo model. The entered data are then used by the computer to calculate corrections to the orientation elements of both photographs for the establishment of absolute orientation.

Three or more control points must be used. The first point should always be the point nearest the center of the array of control points. If more than three control points are used, the model will be oriented to achieve a least-squares error adjustment from the points used.

Individual push buttons are used to identify control points. When these push buttons are activated, the coordinates of control points are entered by using the Data Entry Replace Switch for activating the model point selection switch X_m, Y_m and Z_m. Then by depressing the Compute push button the computer will automatically establish the required corrections in all the orientation elements.

Plotting

Plotting is also controlled in part by the computer program. The constants S_x and S_y are scale factors required by the coordinatograph program to magnify the data for plotting. These entered

S_x and S_y values will cause a movement in the coordinatograph proportional to the change in S_x and S_y, which affect only the horizontal scale for plotting and not the elevations in the model. Figure 7 demonstrates the orientation system for the AP/C. The data used in generating the models are available in the Branch of Astrogeology.

SUMMARY AND RESULTS

Anaglyphic Stereo

Figures 8-11 represent the entire productive effort in terms of generated form-line base maps. This does not, however, reflect the number of repetitive stereo models that were set for attempted definition of absolute orientation. Ranger VIII FA2-3 was, in fact, set up some nine times varying the procedure in three cases. At no time were models reproduced that agreed in essence with another model.

It was noted during these attempts that the assumed datum tilted differently every time and that supposed refinement of parallax and deliberate introduction of various projector rotational motions had little or no effect upon the datum tilt. The conclusion was that lack of definition (image contrast) in conjunction with postage-stamp-size stereo area and narrow angle ray intersection results in a fluid type viewing datum. Experiments with conventional vertical photography where the base to height ratio was deliberately reduced somewhat substantiates this occurrence of fluid-type datum where different parallax solutions tend to have small effects on datum tilts.

Analytic Plotter

The entire effort on the AP/C was limited to crater measurement, spot elevation recording for slope computation, and delineation of geologic units. The operators felt that if time had been available form-line maps could have been produced. For example, Ranger IX FA frames 4-5 were oriented both relatively and absolutely by different operators working independently and

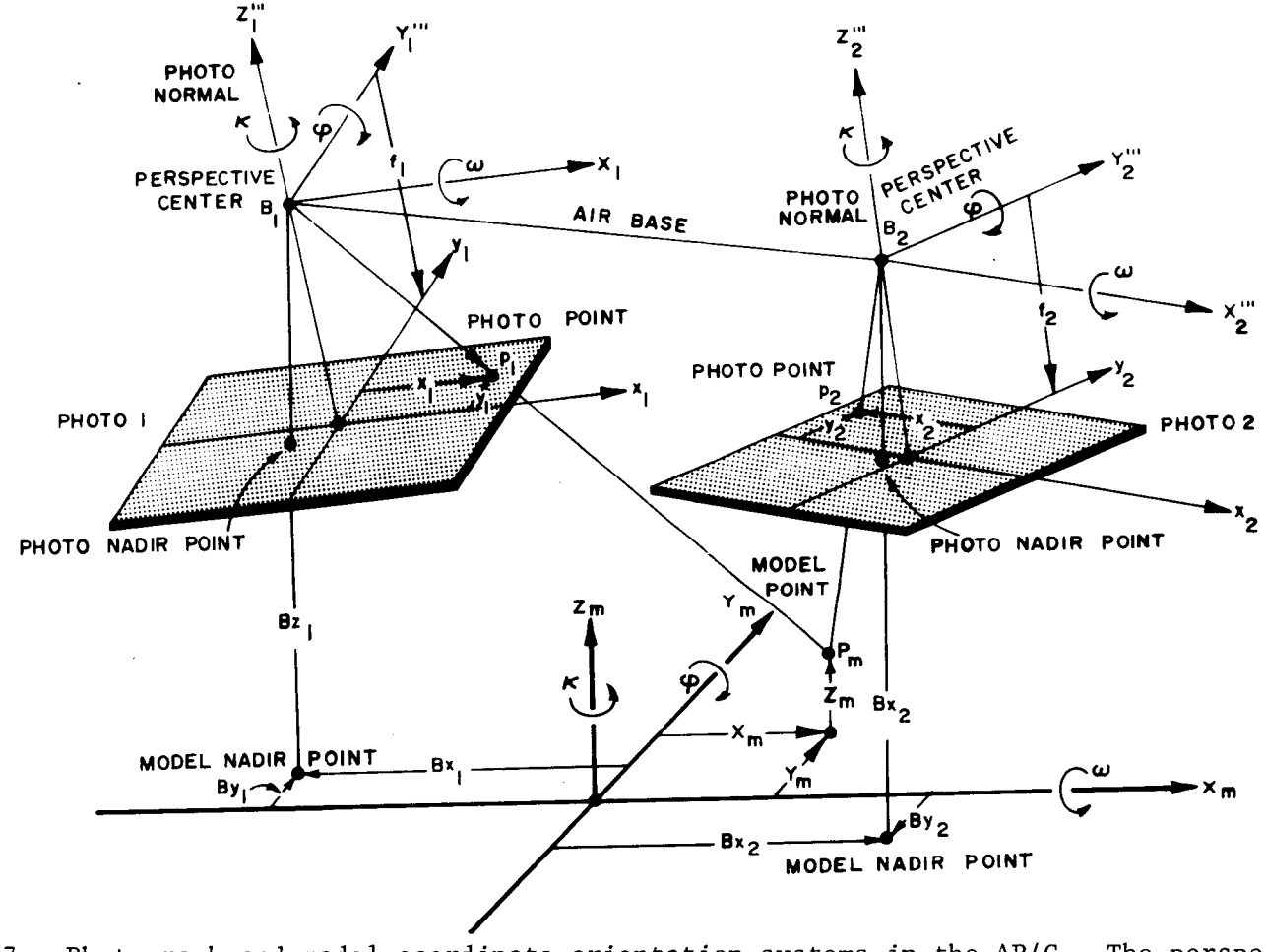

Figure 7.--Photograph and model coordinate orientation systems in the AP/C. The perspective centers are the models locations of the successive camera exposure stations.

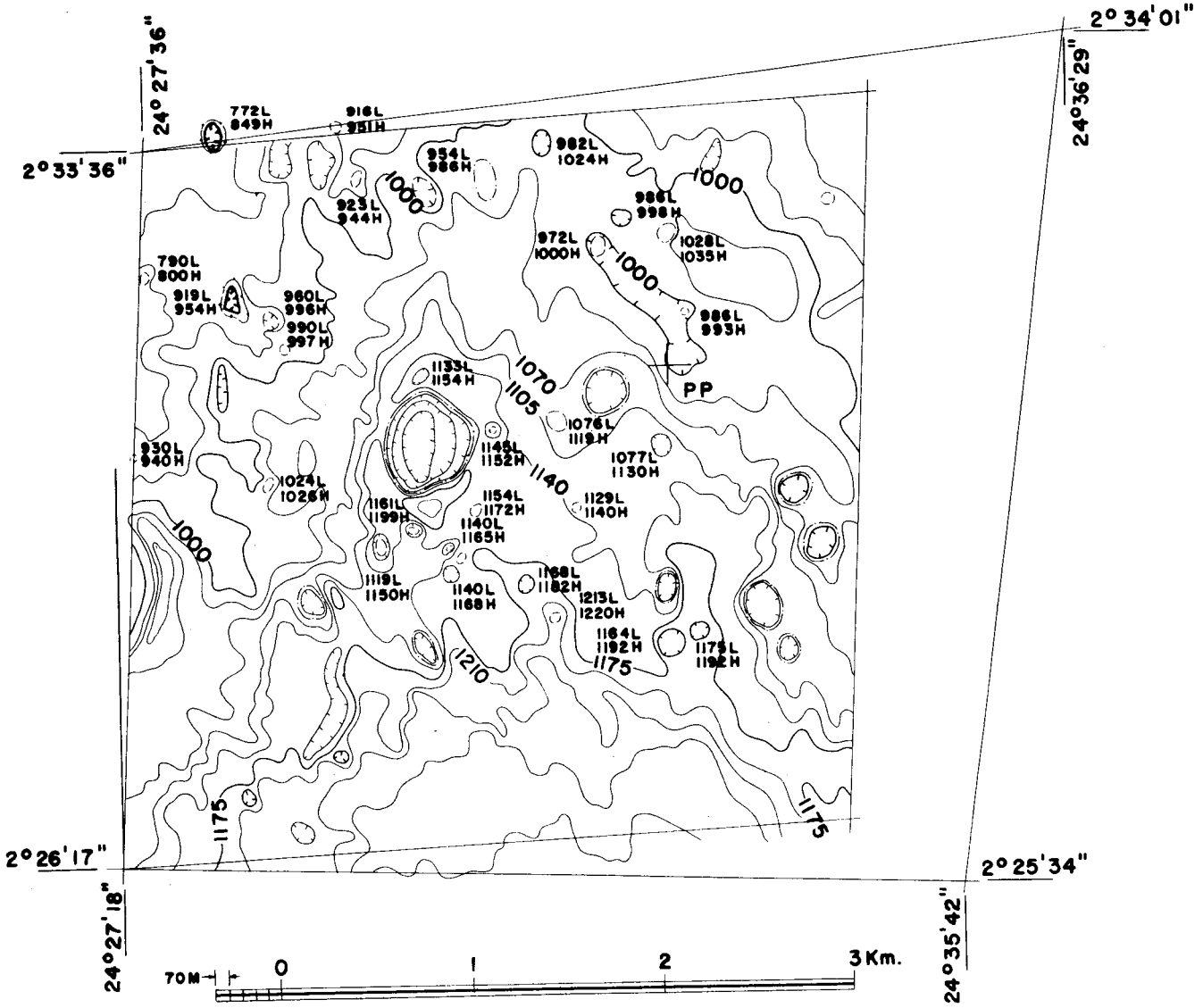
2°34'01"
24°36'29"
24°27'36"
2°33'36"
772L 849H
916L 951H
954L 986H
982L 1024H
923L 944H
1000
988L 998H
1028L 1035H
972L 1000H
790L 800H
919L 954H
960L 996H
990L 997H
986L 993H
PP
1133L 1154H
1070
1105
1076L 1119H
1077L 1130H
930L 940H
1148L 1152H
1140
1024L 1026H
1161L 1199H
1154L 1172H
1129L 1140H
1140L 1165H
1119L 1150H
1140L 1168H
1168L 1182H
1213L 1220H
1164L 1192H
1175
1179L 1192H
1210
2°26'17"
24°27'18"
2°25'34"
24°35'42"
70M
0
1
2
3Km.

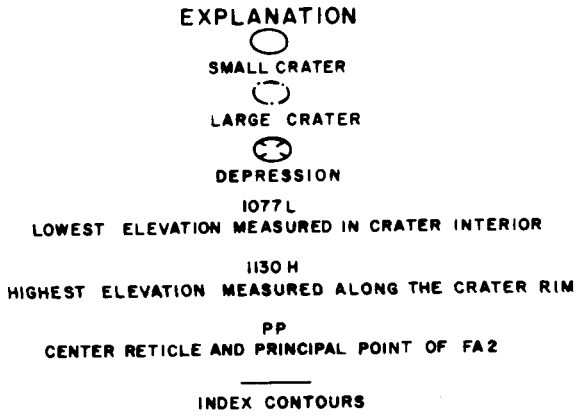

Figure 8.--Form-line base map compiled from Ranger VIII FA2 and FA3 photographs. Compiled by ER55. Absolute orientation was obtained through close approximation of horizontal on lunar coordinate of reticles whose data are furnished by Jet Propulsion Lab., Pasadena, Calif. Arbitrary datum plane contains principal point of FA3 at assigned elevation of 1,000 meters. Contour interval 35 meters.

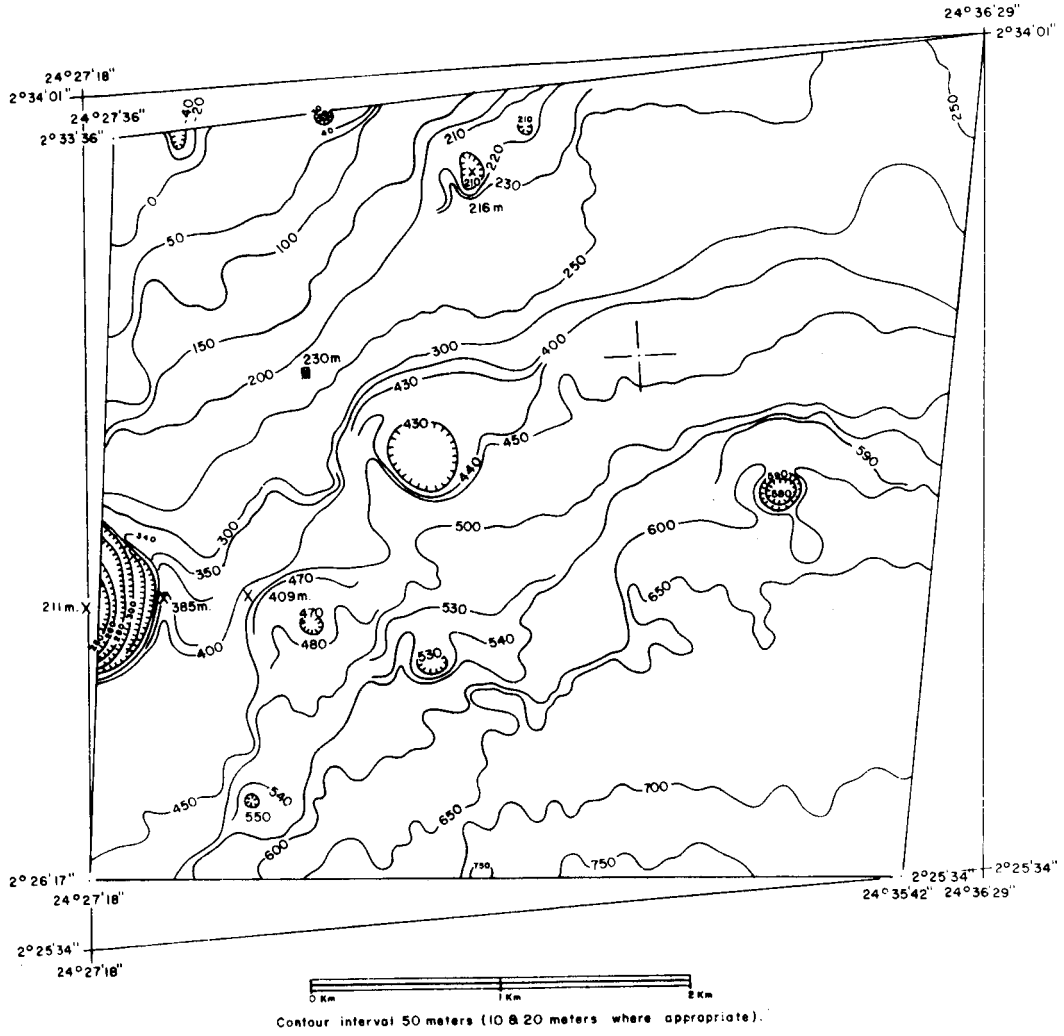

Figure 9.--Form-line base map compiled from Ranger VIII FA2 and FA3 photographs. Compiled by AP/C.

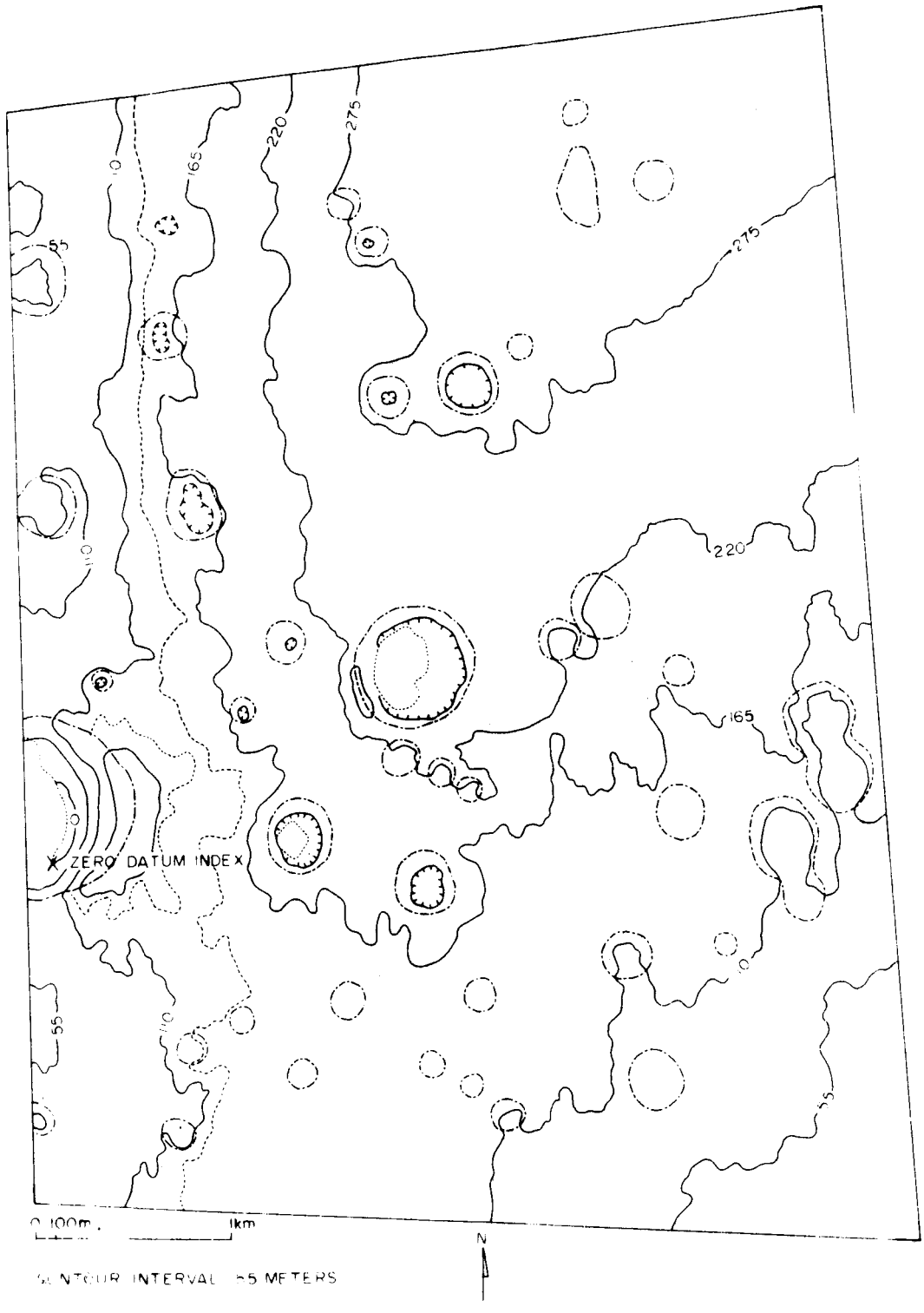

Figure 10.--Form-line base map compiled from Ranger VIII FA2 and FA3 photographs. Compiled by AP/C.

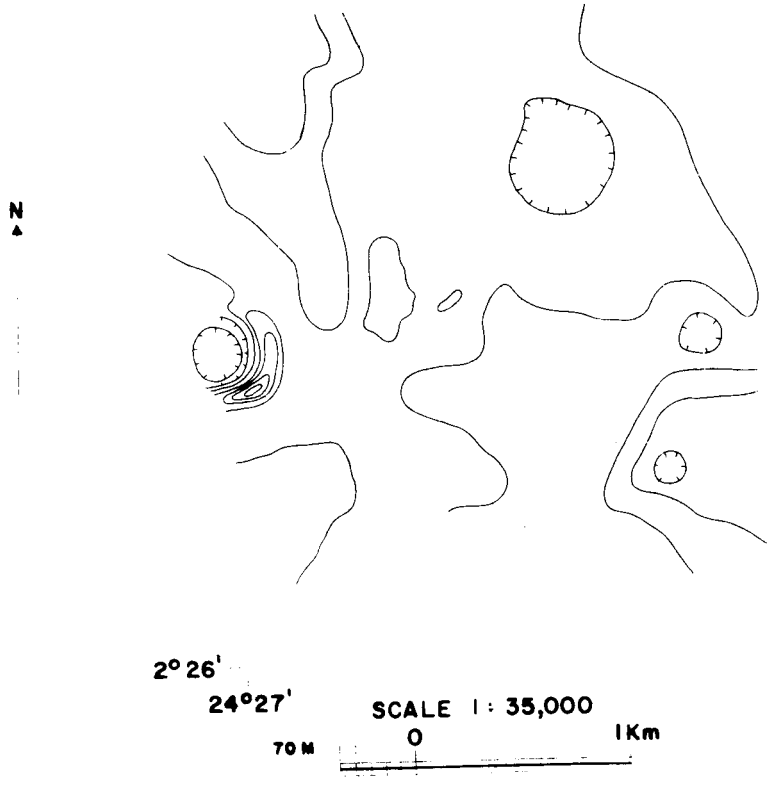

Figure 11.--Sketch map of Ranger VIII FA frames 2-3 drawn from spot elevations derived from AP/C.

the results varied only within a few microns.

Figure 11 is a rough sketch map of Ranger VIII FA frames 2-3 drawn from spot elevations. Comparison of figures 9 and 11 indicates that a reasonable agreement exists in the topographic forms derived by the ER55 and AP/C model generations. The subtle similarities would definitely suggest a true stereo model.

The following models were set on the Ohio State Highway Department's AP/C at Columbus, Ohio.

Ranger VII FA frames

1-2 Image match poor. Parallax residuals up to 200 microns. No measurement made.

3-4 Datum appeared erratically warped. Shadow lengths would not agree with crater wall slope measurements. Very weak viewing datum.

Ranger VIII FA frames

2-3 Model set twice with residual parallax, after absolute orientation, less than 5 microns in both cases. Shadow lengths in agreement with measured slopes. Heighting repeatability within 10 microns on specific image points. A very good model overall. Datum appeared very reasonable and no warpage apparent. Viewing datum appeared relatively solid.

3-4 Parallax residuals less than 20 microns. Shadow lengths in agreement with measured slopes. Time element eliminated further investigation. Fair viewing datum.

Ranger IX FA frames

4-5 Parallax residuals 10 microns after absolute orientation. Extensive heighting measurements made. Shadow lengths in agreement with measured slopes. The best viewing datum of all Ranger models tested.

1-2 Parallax residuals 300 microns. Datum tilts excessive. Viewing datum fluid.

In general, it was concluded that viewing on the AP/C was contingent in part upon the degree of contrast of the diapositive as related to definable image points. Only a trial-and-error

method of diapositive making was applicable as no one factor such as dark or light diapositives would suffice for various frame combinations.

REFERENCE

Heacock, R. L., and others, 1966, Ranger VIII and IX, pt. 2, Experimenters' analyses and interpretations: California Inst. Technology, Jet Propulsion Lab., Tech. Rept. 32-800.

INTERPRETATION OF SMALL LUNAR CRATERS

By H. J. Moore

INTRODUCTION

The successful operation of the Ranger, Luna 9, and Surveyor I spacecraft has provided excellent photographic data on the fine-scale features of the lunar surface. These features are predominantly craters, although blocks and other positive features are present. The origin of these features is discussed herein, and man-made craters are compared with small lunar craters, thereby enabling inferences regarding the physical properties of the lunar surface.

All the data on craters produced by experimental impact in the laboratory were collected as part of a cooperative program of research between the U.S. Geological Survey and Ames Research Center, Moffett Field, Calif., where the principal experimenters are D. E. Gault, W. R. Quaide, and V. Oberbeck. Data on missile impact craters were collected through the courtesy of the U.S. Army and the Commanding General of White Sands Missile Range, N. Mex.

PREDICTED DISTRIBUTION OF CRATERS ON THE LUNAR SURFACE

Calculations of the frequency distribution of impact craters produced by the influx of meteoroids and other objects from space suggest that the lunar surface should reach a "steady-state" (Moore, 1964; Shoemaker, 1965, p. 122-124) and become almost completely covered with small impact craters of various sizes. In this "steady-state," craters are destroyed as rapidly as they are formed so that the general appearance of the surface remains the same, although the details continually change with time. The "steady-state"

is first attained for the smallest craters and with time extends to the larger ones.

One set of calculations (Moore, 1964) is based on the assumption that the cumulative frequency of meteoroids and other objects from space that impact the lunar surface is inversely proportional to their masses (see Whipple, 1963, curve B) and then uses cratering theory to establish the size of craters produced. Calculations using Whipple's curve B lead to the conclusion that the lunar surface cannot contain the number of craters that would eventually be formed on it. Hence, craters must be destroyed by subsequent impacts. Assuming that the lifetime of a crater is proportional to its linear dimension, the calculations suggest that the cumulative-frequency distribution of craters on the lunar surface would be composed of two parts. The cumulative frequency of the smaller craters, where the "steady-state" has been achieved, should be inversely proportional to the square of their diameters; and the cumulative frequency of the larger craters, where the "steady-state" has not been achieved, should be inversely proportional to the cube of their diameters. For a billion-year-old surface, 10 to 34 percent of the area should be covered by craters within each decade of crater diameters from 0.0001 to 10 m and possibly to 100 m across. For this "steady-state," the craters in each of the size intervals would range from fresh and unmodified to partly destroyed by erosion and infilling (see also Jaffe, 1965). For the condition of 10 percent coverage of the surface by craters in a given decade of crater diameters, the craters range from fresh craters to those about 3/10 of the way to destruction. For the condition of 34 percent coverage of the surface, the craters range from fresh to barely discernible. Erosion of the craters results from the ejection of debris during crater formation by subsequent impacts. Infilling results as material dislodged by impact moves downslope and collects in depressions.

Similar crater distributions might also be produced by the impact of fragments along rays radiating from craters such as Copernicus, Tycho, or Aristarchus (Moore, 1964, p. 49; Shoemaker 1965) as well as around young smaller impact craters.

Predicted crater frequencies and actual crater counts made from photographs of the lunar surface are compared in figure 1. The predicted crater distribution will be compared with that of the lunar surface later.

EXPERIMENTAL SIMULATION OF LUNAR CRATERS

The U.S. Geological Survey and Ames Research Center (NASA) have conducted a cratering experiment in the laboratory as part of a cooperative program of research. The experiment illustrates how repeated impacts produce a "steady-state" surface and what crater morphologies may be expected for a surface that has reached the "steady-state." The surface produced in this experiment was similar to surfaces shown in the highest resolution Ranger photographs and the surface around Surveyor I. These surfaces are characterized by craters of various sizes in various states of preservation.

In the experiment, craters were produced by dropping and firing projectiles into an 8-foot-square box filled to a depth of 30 cm with noncohesive sand covered by a layer of coarse carborundum powder about 2 cm thick. The projectiles, the method of projection, the average diameters of craters produced, and the relative frequencies of impact are as follows:

Projectile	Projector	Average crater diam. (cm)	Relative projectile frequency
30 cal	rifle, 30-06	30	1.0
22 cal	rifle, 22	13	10.4
BB	BB gun	4.2	106
Birdshot	rifle, 22(sawed off)	2.5	1,410
#8 shot	25-foot drop	1.1	11,200
#12 shot	25-foot drop	.52	127,000

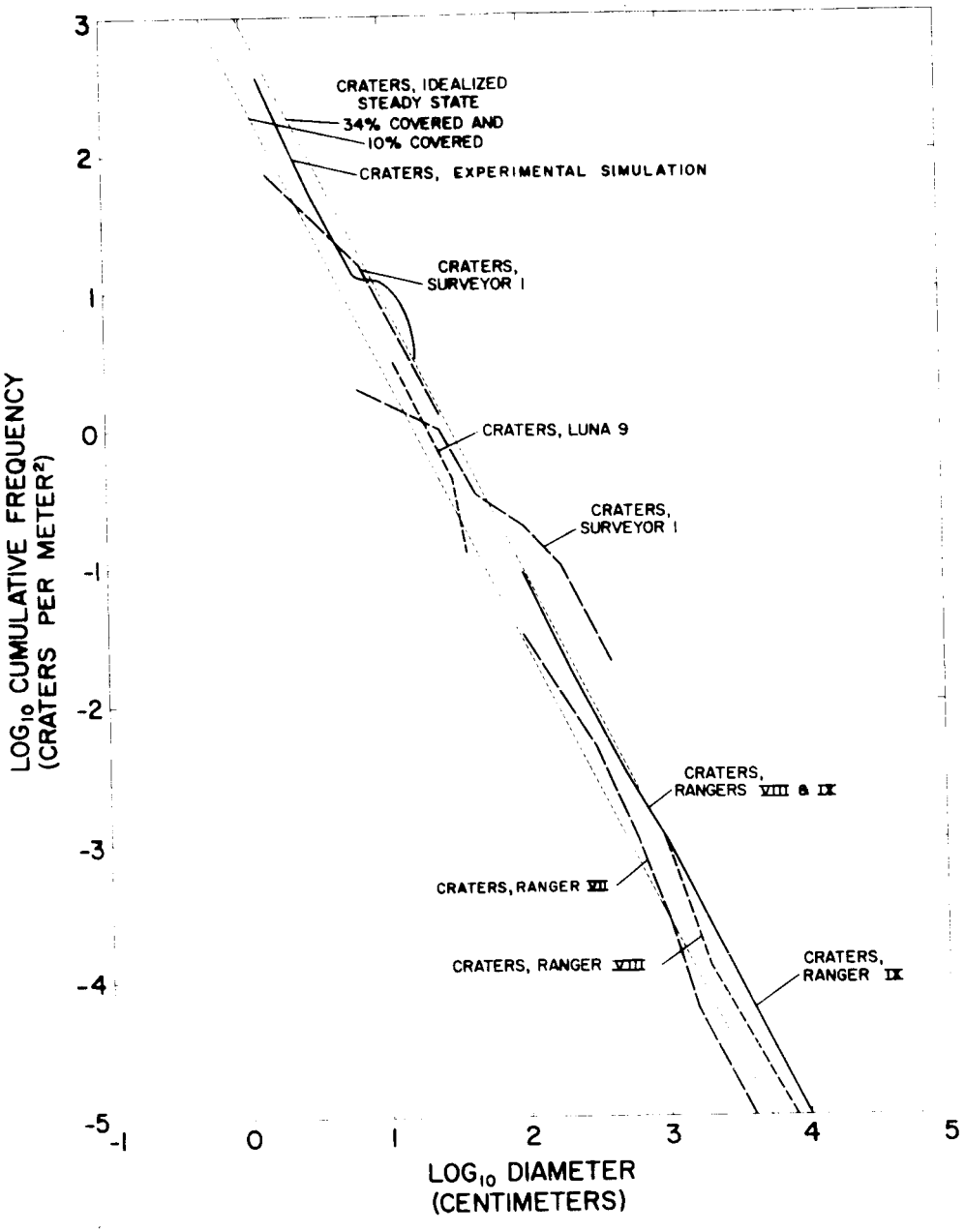

Figure 1.--Frequency distribution of small craters on the lunar surface and predicted frequency distribution and experimental simulation.

The 30-caliber, 22-caliber, and BB projectiles were fired at random points using a grid to control aiming. The sequence of firing was not random; one 22-caliber bullet was fired after every ten BB's, and one 30-caliber bullet was fired after every ten 22-caliber bullets. Precise sequencing of birdshot and drops of #8 and #12 shot was not possible since about 5, 13, and 153 craters per square foot were produced by each firing or drop of birdshot, #8 shot, and #12 shot, respectively. The calculated number of BB's and shot fell only into the central 4-foot square because of the large number of shot required. According to the calculations of Moore (1964), the product of the relative frequencies of the craters produced in each size class and the cube of their diameters should be constant. The list above shows that this was nearly achieved; however, the craters produced by the BB's were about 20 percent too small--hence the bend in the crater frequency curve (fig. 1). The most significant shortcoming of the experiment is the small range of sizes of craters produced. On the lunar surface, craters range in diameter from less than a few centimeters to more than hundreds of meters, whereas the craters in the simulation range from 0.5 to 30 cm.

In spite of the small range of sizes of craters produced and the under-size BB craters, the experiment was instructive. The initially smooth surface soon became pocked with craters of all sizes as the firing proceeded. In the early stages, areas between the smallest craters were smooth and flat where no craters were present. With continued bombardment the surface reached a "steady-state" for the smaller craters and none of the original surface escaped the bombardment. Upon reaching the "steady-state," craters were produced approximately as rapidly as they were destroyed. Further bombardment eventually produced a "steady-state" for all sizes of craters. When the surface reached the "steady-state," the general appearance remained essentially the same with continued bombardment although the details of the surface continually changed.

Craters were destroyed by a combination of erosion and infilling, as illustrated in figure 2. Two young craters with virtually no superposed smaller craters can be seen. The ejecta from these craters has infilled and buried many smaller craters around them, and a large number of smaller craters were destroyed by the excavation. In the lower right-hand corner of figure 2, the ejecta blankets of two fairly fresh craters have been somewhat eroded by smaller craters. Many rimless craters are visible whose ejecta blankets are so eroded by impacts producing smaller craters that they are no longer discernible. Additional shallow depressions with virtually no shadows in them may be seen. Some of these depressions represent craters on the verge of being completely obliterated.

The craters on the experimental surface can be grouped into morphologic stages, like those of terrestrial features (see for example, Davis, 1909, p. 170, 176-178): youthful to old. Youthful craters are well defined and have distinct rims and ejecta blankets. Old craters are vague rimless depressions. Such stage designations do not indicate absolute ages but rather relative ages of craters the same size. Crater counts made by N. J. Trask from a photograph of the central 4-foot square of the final surface are shown in figure 1. The final surface will be compared with the lunar surface later on. It is also noteworthy that many of the larger craters have smaller craters on their rims, and occasional doublets are found among the intermediate-size craters. Other craters appear to be alined.

MISSILE-IMPACT AND EXPLOSION CRATERS

Ejecta and morphologies of experimental craters reflect the properties of the materials in which the craters formed. The nature of these properties may be revealed by: 1) the presence of large blocks in the ejecta, which represent unfractured cohesive materials, and the presence of small blocks, which may represent intensely fractured rocks or fragmental materials with low cohesion;

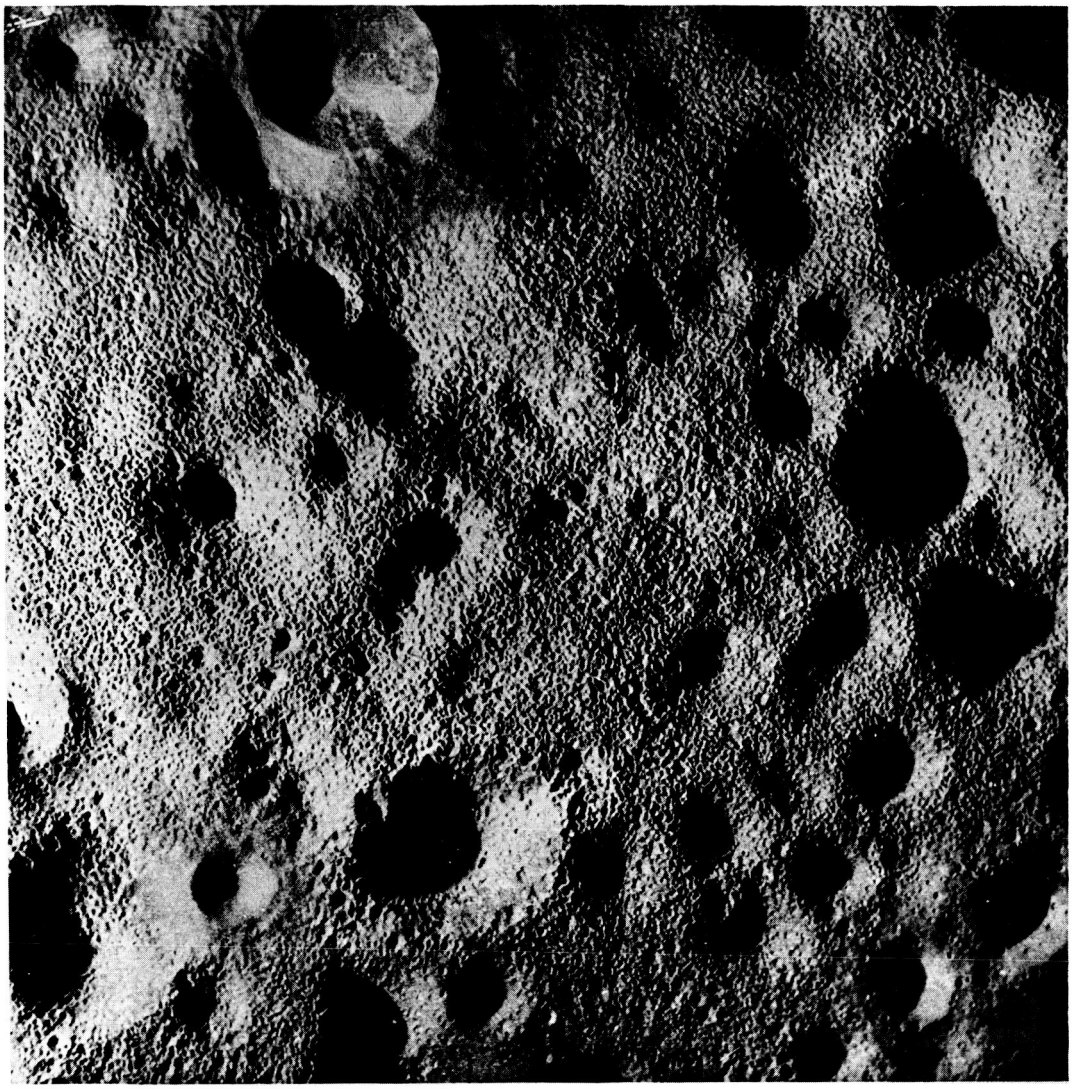

Figure 2.--Photograph of experimental simulation of lunar surface illustrating erosion and infilling of craters by projectile impacts. Note the various stages of preservation--from fresh-appearing craters with rims to those barely discernible. Largest crater is about 30 cm across.

2) crater-wall slopes--slopes of more than about 60° indicate cohesive rocks and slopes between 25° to 40° imply little or no cohesion; 3) crater rims--where craters less than a meter or so across have smooth, continuous, elevated rims completely surrounding them, little or no cohesion is indicated; and 4) crater outlines--a round outline indicates low cohesion if the projectile was not irregular in shape and its trajectory was oblique.

Current data on experimental impacts in natural materials cover craters so small they are measured in microns and craters as large as 8 m across. However, the lunar photographs in this report show craters that are as much as tens of meters across. The only man-made craters with which large lunar craters can be compared are those produced by explosives. Morphologic comparison of craters produced by experimental impact and craters of comparable size produced by explosion indicates that extrapolation can be made provided that the scale depth of burial of the explosive[1] is less than 1.50 ft per $lb^{1/3}$ TNT equivalent (Moore and others, 1964). For explosives detonated above the surface or at greater scaled depths, the comparisons are no longer valid.

The ejecta around craters produced by chemical explosives buried at shallow depth in uniform flow basalt at the Nevada Test Site is marked by the profusion of conspicuous blocks that is characteristic of materials with high cohesion and widely spaced fractures (see Vortman and others, 1962, p. 236-243, figs. A1-A8; Polatty and Curry, 1964, photos. 1-13; and Moore, 1966, p. 268, fig. 12). In materials like the flow basalt, 4 m blocks may be found around craters 67 m across; 2.4 m blocks around craters 29 m across; and 1.5 m blocks around craters 10 m across. There is also a great profusion of blocks 0.3 m across, and larger, to distances exceeding one crater diameter.

---

[1]The scale depth of burial used here is equal to the depth of burial of the explosive in feet divided by the cube root of the TNT equivalent of the explosive in pounds.

Studies of craters produced by missile impacts at White Sands Missile Range yield the same result--large blocks are abundant around craters in materials with sparse fractures and high cohesion (Moore and others, 1964b and unpub. data). Figure 3 shows an impact crater produced in indurated gypsum by a missile with a trajectory near 45° to the ground surface. Shear-vane measurements indicate that the unconfined compressive strength of the gypsum is between 3.0 to 6.0 bars.

Blocks are scarce or absent around craters in intensely fractured materials and in weakly cohesive to cohesionless fragmental aggregates. Craters 8-9 m across produced by 256-pound chemical explosive charges buried at shallow depths in alluvium illustrate this (see Murphy, 1961, p. 39, figs. A22-A24; Vortman, 1966, p. 34 and 36, figs. A1, A2). Ejecta around these craters is hummocky with radial ridges, broad gentle hills, and rare blocks. Ejecta around missile impact craters near 6 m across in alluvium is similar to that around explosion craters (see fig. 4). Again, radial ridges, broad gentle hills, and rare small blocks characterize the ejecta.

The character of the ejecta from craters about 1 m across and smaller is similar to that of larger craters. Ejecta from impact craters and explosion craters produced in dry sand is free of large fragments; however, clods occur in ejecta from craters in weakly cohesive materials, such as wet to moist sand and weakly bonded sand. These may be as large as 0.10 crater diameters for craters 5 to 20 cm across (see for examples, Fulmer, 1965; Gault and others, 1966b). Ejecta from craters in unfractured cohesive materials is characterized by scattered fragments in and around the crater. Lengths of such fragments may be as much as 0.1 to 0.3 crater diameter for craters up to a meter across (Gault and others, 1966b).

The order of deposition of ejecta from projectile impact craters and explosion craters is the reverse of the vertical sequence of undisturbed target materials. Thus, debris from the

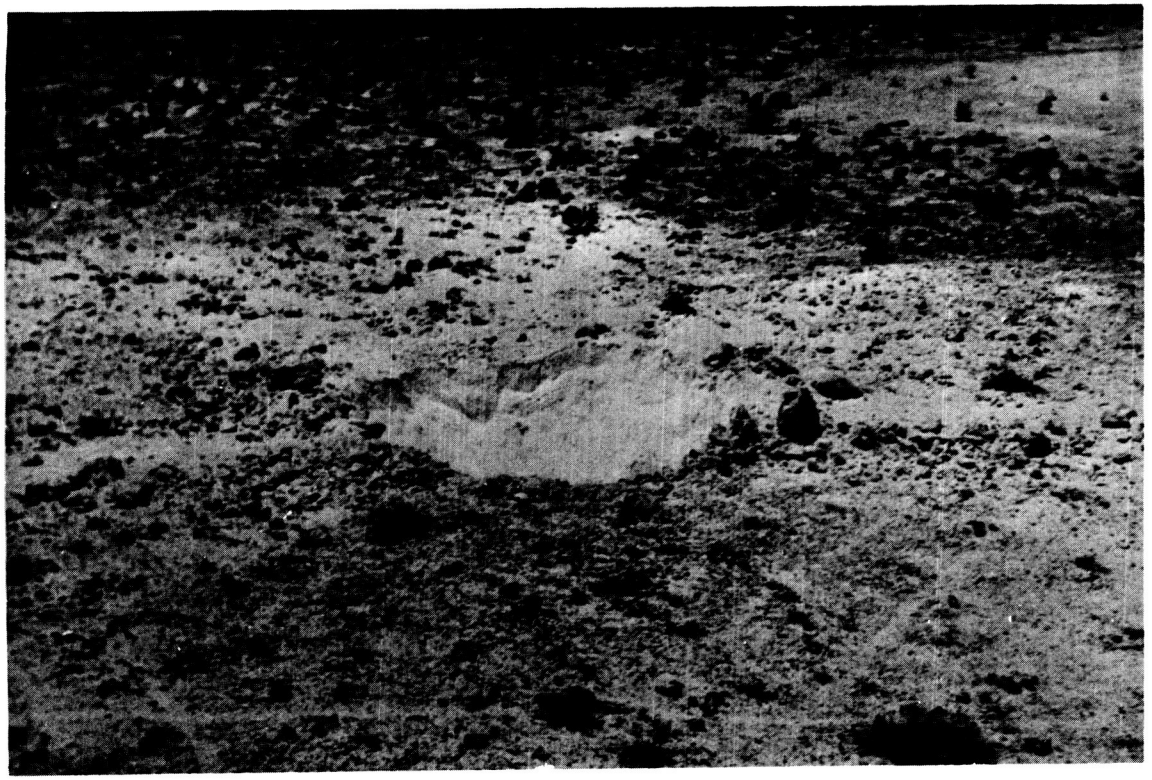

Figure 3.--Crater produced by missile impact in indurated gypsum. Crater is about 6 m (20 ft) across and 1.5 m (5 ft) deep. Blocks on rim are as long as 1 m (3.3 ft) and as wide as 60 cm (2 ft). Many smaller blocks are present. (Oblique aerial photograph courtesy of U.S. Army).

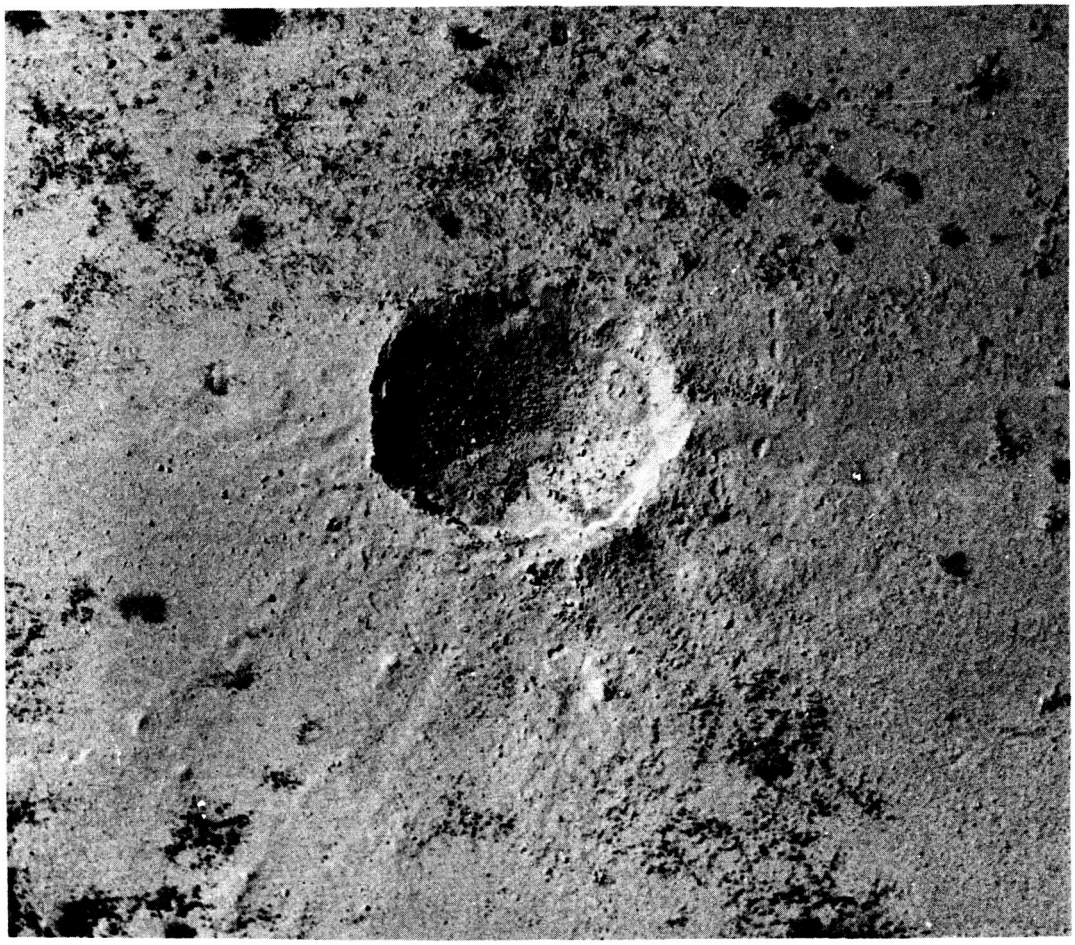

Figure 4.--Crater produced by missile impact in gypsiferous alluvium. Crater is about 6 m (20 ft) across and 1.5 m (5 ft) deep. Note steep crater walls, paucity of blocks, and asymmetrical ejecta resulting from the oblique trajectory. The trace of the path of the missile is from top to crater. (Nearly vertical aerial photograph courtesy of U.S. Army).

lower layers of the target material occurs at the surface of the ejecta blanket superposed on ejecta from higher layers (Shoemaker, 1960; Moore, 1964). This relationship is shown in figure 5 where fragments from a lower layer of cohesive silty clay rest on very fine ejecta from weakly cohesive to cohesionless sand and silt from the upper layer. The crater in figure 6 was produced exclusively in the cohesive layer of silty clay. The profusion of blocky ejecta is characteristic of the more cohesive silty clay. The craters in figures 5 and 6 are both the same size and were produced by missile impacts.

Walls of craters produced by projectile impacts vary in slope depending on the cohesion of the material and the size of the crater. Slopes of crater walls in cohesionless fragmental materials are near the angle of repose of the material--30° to 40°--regardless of the size of the crater. In cohesive materials the mean slope of craters 30 m across and larger may be near 30° or 40° but locally slopes may be 60° or more (see fig. 4). Craters less than 0.3 m across in porous cohesive materials such as pumice have very steep walls, but their depth to diameter ratio may exceed 1.0 (see for examples, Gault and others, 1966b; and Moore and others, 1964a). Slopes of walls of very small craters in hard, dense rocks such as basalt may not be significantly different from those of craters in sand. Similarly, depth to diameter ratios of small craters in either basalt or sand may be near 0.25 to 0.20.

Raised rims are typical of all craters larger than 30 to 40 m, but whether or not small craters have raised rims depends on the cohesion of the target materials. Craters less than 1 m across in pumice, basalt, granite, and other strong cohesive materials are almost always rimless, whereas those in materials like weakly bonded sand, wet sand, and dry sand are surrounded by raised rims. Rim height to crater diameter ratios are near 0.025 for small fresh craters in dry sand (see Gault and others, 1966b; and Fulmer, 1965). Rim height to crater diameter ratios may be 0.10, or more, for small fresh craters in wet sand (see Fulmer, 1965).

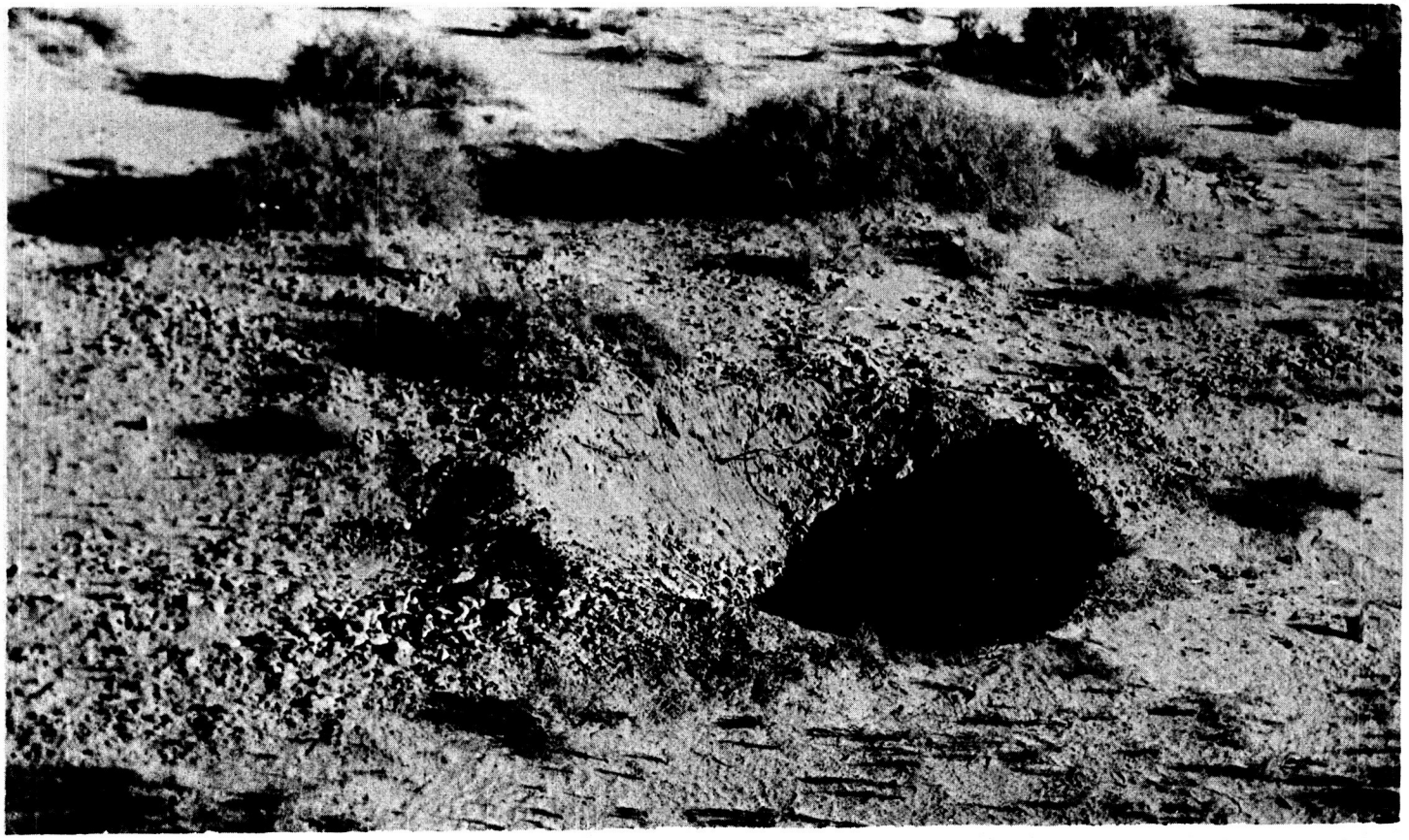

Figure 5.--Missile impact in layered material. Upper layer is very weakly cohesive sand and silty sand. Lower layer is weakly cohesive silt and sand with uniform structure. Crater is about 6 m across. (Oblique aerial photograph courtesy of U.S. Army).

Figure 6.--Blocky ejecta from missile impact crater in uniform cohesive silt and clay beds. Crater, located in upper right-center of picture, is about 6 m (20 ft) across. (Photograph courtesy of U.S. Army).

A smooth, round configuration is typical of small craters produced by equidimensional explosives or projectiles in cohesionless materials. The extent to which the properties of materials affect crater outline decreases with increasing crater size; however, the outlines of even large craters may be affected (Fulmer and Roberts, 1963). The outlines of missile impact craters near 6 m across in indurated gypsum are commonly linear and polygonal, whereas craters in sand are circular to elliptical. Experimental data on shapes of small impact craters have been cited previously (Gault and others, 1966a).

In summary, fresh craters less than about 1 m across in dry noncohesive materials such as sand are characterized by a round outline, the absence of large fragments in the ejecta, crater walls with all slopes near the angle of repose of the material, and smooth continuous elevated rims. Fresh craters less than 1 m across in very weakly cohesive materials such as moist sand are characterized by a round outline, clods in the ejecta, crater walls with average slopes near 30°-40°, and continuous elevated rims. Craters less than 1 m across in cohesive dense indurated materials such as granite, sandstone, and flow basalt are rimless and large fragments are scattered in and around them. Craters in porous cohesive materials such as pumice are steep walled and rimless. Large blocks and locally oversteepened crater walls are characteristic of large craters (up to 100 m) in sparsely fractured cohesive materials, whereas smooth ejecta blankets without abundant blocks and smooth walls with slopes of 30°-40° are characteristic of fresh large craters in noncohesive to weakly cohesive materials.

DATA FROM RANGER IX, LUNA 9, AND SURVEYOR I

Crater Distribution

The successful lunar probes Ranger IX, Luna 9, and Surveyor I have transmitted extensive data on the lunar surface. Most of the data that the probes collected were photographic, but Surveyor I

also obtained information on the mechanical properties of the lunar surface. Photographs taken by all the probes show that the fine-scale topography of the lunar surface is dominated by craters, but positive features such as blocks, fragments, and clods become increasingly abundant with increasingly finer scale, until, at a scale of a few centimeters, they are common features of the lunar landscape.

The highest resolution photographs taken by Ranger IX (California Inst. Technology, 1966, pls. A-70, B-88, and P-12) show that in degree of preservation, lunar craters 3 to 600 m wide vary from fresh to subdued. Craters of a given size may have well-defined rims and sharp internal shadows or subdued rims and diffuse internal shadows, or they may be rimless depressions with almost no internal shadows. Surfaces around Surveyor I (Jaffe and others, 1966) and the Soviet Luna 9 (Akad. Nauk SSSR, 1966) are similar to those photographed by Ranger IX but craters are smaller--a few centimeters to several meters in diameter. The continuous sequence of crater morphologies--from sharp craters with well-defined rims to rimless shallow depressions--is present on these surfaces. The cratered surface around Surveyor I is shown in figure 7.

From photographs by Ranger VIII and IX (Trask, 1966), Luna 9 (Akad. Nauk SSSR, 1966) and Surveyor I (Morris, E. C., 1967, personal commun.), it has been determined that the frequency of craters per unit area increases rapidly with decreasing crater size. The cumulative frequencies of smaller craters (see fig. 1) appear to be nearly proportional to the reciprocal of the square of the crater diameters, with the exception of the larger craters counted around Surveyor I. However, it should be noted that the counts for large craters at the Surveyor I site may be revised on the basis of Lunar Orbiter II data (Morris, E. C., 1967, personal commun.).

In contrast with Ranger photographs, both Luna 9 and Surveyor I photographs show a substantial number of positive morphologic forms because of the increase in the frequency of blocks, fragments,

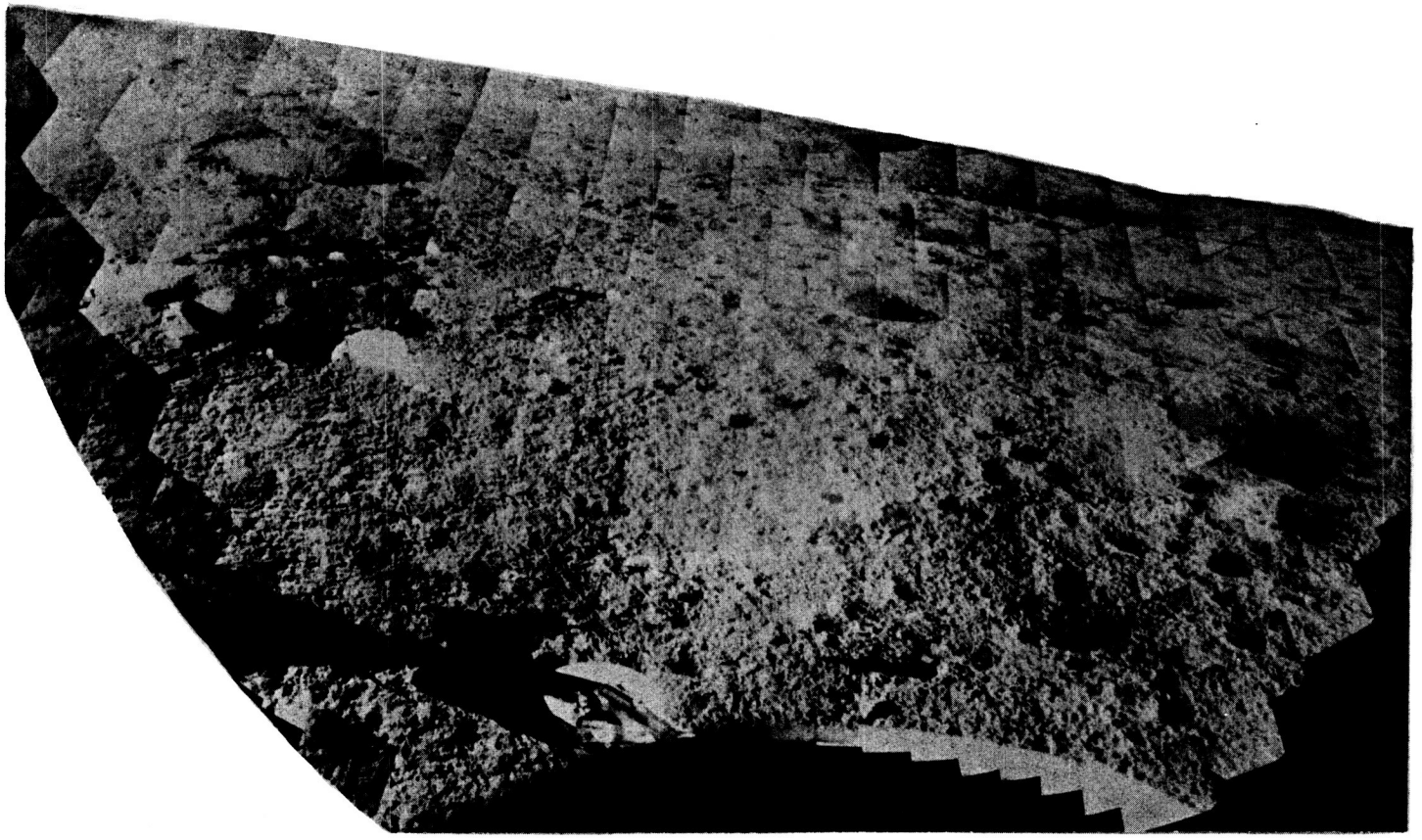

Figure 7.--Mosaic of photographs of lunar surface taken by Surveyor I. Rimmed crater in upper left is between 2 and 3 m across. Footpad in foreground is about 30 cm across.

and clods with increasingly finer scale. Such an increase in frequency with decreasing size is borne out by unpublished studies (Morris, E. C., 1967, personal commun.) which indicate that the cumulative frequency of blocks and fragments is inversely proportional to the 2.2 power of their diameters. Both U.S. and Soviet observers report that fragments, like craters, vary in form. Forms range from angular to rounded.

Description of Selected Lunar Craters

Certain lunar craters were selected for description here: 1) craters similar in size to man-made craters, 2) craters apparently unmodified in form, and 3) craters that penetrate only the uppermost layers.

The last partial frame from the Ranger IX B camera (fig. 8) shows craters from 25 m down to 1 m across. Craters 1 m and wider shown in this photograph are generally surrounded by distinct raised rims; of the craters smaller than 1 m that are visible, some are rimmed, some are rimless. The areas around the raised rims of the three largest craters in figure 8 are relatively smooth, although a few craters and positive equidimensional features are present. The sun angle is only 5°, but the sparse positive features cast weak short shadows. There is no evidence for steep slopes in the upper walls of the craters shown in Ranger IX photographs.

Small craters photographed by Surveyor I are similar to those of comparable size photographed by Ranger IX. Several craters between 0.7 and 3.3 m across with smooth raised rims and gently sloping walls occur around Surveyor I (fig. 7 and Jaffe and others, 1966a, p. 35-39). Many of the smallest craters, a fraction of a meter across, also have distinct rims and gently sloping walls. Lumps measuring as much as 1/5 to 1/40 of the crater diameter are common around the rims of the smallest craters. A few fragments are scattered around one crater about 6.3 m across, and blocks are abundant in the ejecta around a crater about 30 m across (Jaffe and others, 1966a, fig. 111-10, p. 19 and fig. 111-24, p. 39).

Figure 8.--Last partial frame from Ranger IX B camera. Largest crater is about 25 m (82 ft) across. Next largest craters are about 13 m across. Craters as small as 1 m across are clearly visible.

Most of the blocks around the 30 m crater are angular with smooth faces and some are rectangular.

Rimmed craters similar to those photographed by Surveyor I also appear in the Luna 9 panoramas (Akad. Nauk SSSR, 1966). The clearest examples of rimmed craters are about 20 to 30 cm across, but many rimmed craters less than 20 cm are present. Most rim heights are near 0.13 times the crater diameter, and a depth-to-diameter ratio near 1/4 was measured on one 21 cm crater whose floor is visible. The rims of the craters are marked by lumps about 0.13 times the crater diameter.

In summary, fresh-appearing lunar craters near 10-20 m across have raised rims and smooth ejecta blankets with few positive features; smaller lunar craters--near 3 m across--are circular with smooth raised rims. Craters around 20 cm across have lumpy raised rims. None of the smaller craters have steep crater walls.

INTERPRETATION OF LUNAR PHOTOGRAPHIC DATA

Crater Distribution

The size-frequency distribution and morphologic variation of small lunar craters shown in the highest resolution photographs by Ranger IX, Luna 9, and Surveyor I broadly fulfill the expectations of the concept of a "steady-state" cratered surface produced by repeated impacts of meteoroids and other debris from space. In any size group there is a continuous morphologic series: fresh-appearing craters with well-defined rims grade into shallow craters with subdued rims, which grade into nearly obliterated craters. Such variations are in substantial agreement with the theoretical predictions of crater aging on a constantly bombarded surface and with experimental simulation. This conclusion is substantiated by comparing vertical and oblique photographs of the experimental surface (figs. 2, 9) with photographs of the lunar surface (figs. 7, 8; also see Calif. Inst. Technology, 1966, pl. A-70). In addition, crater counts made using Ranger

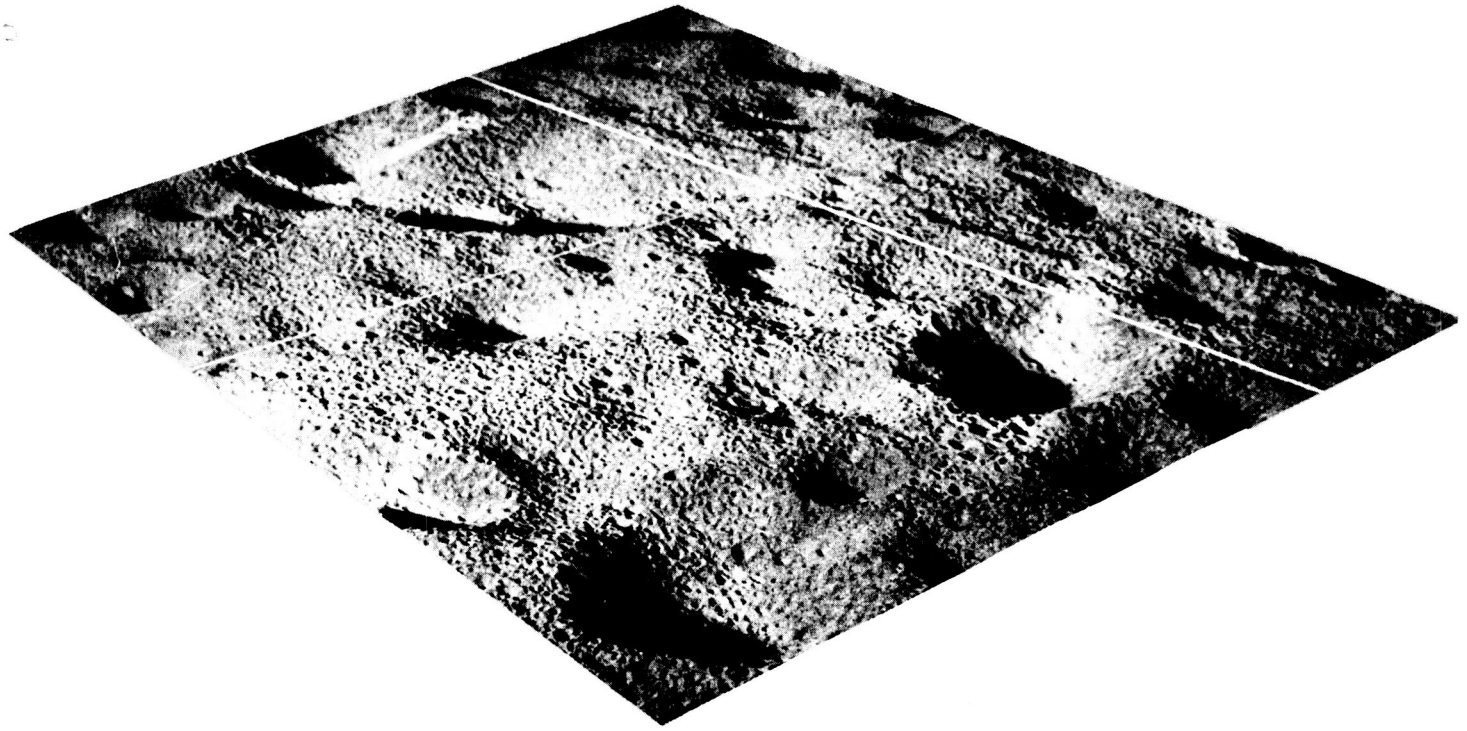

Figure 9.--Oblique photograph of surface produced during experimental simulation.

photographs (Trask, 1966), Luna 9 panoramas (Akad. Nauk SSSR, 1966), and Surveyor I photographs (Morris, E. C., 1967, personal commun.) are similar to those predicted for the lunar surface (Moore, 1964) and those of the simulated surface (Trask, 1966, personal commun.). The size-frequency distributions of craters on those surfaces are shown in figure 1. There are significant differences between predicted, experimental, and actual crater frequencies, but they can be explained. Steep slopes (> -2.0) of the frequency distribution for large craters imply that the "steady-state" has not been reached for the large crater sizes. Separations of the various curves may be related to differences in visibility and resolution caused by different illumination angles and different viewing angles of the photographs. Frequencies of the very small craters around Luna 9 and Surveyor I are in good agreement with the "steady-state" expectations, but the largest craters photographed by Surveyor I are significantly more abundant. Such an apparent abundance may arise from the inability to measure large more distant craters and areas with the cycloptic Surveyor. Subsequent Lunar Orbiter photographs bear this out. The flexure in the crater count curve for the experimental simulation is due to the fact that the BB projectiles produced craters 20 percent too small for their frequency. It is necessary to stress again that projectiles of only six sizes were used to produce craters in the experimental simulation, whereas the size range of objects that impact the lunar surface is virtually unrestricted. A greater range of small crater sizes in the experimental simulation would soften all features and subdue the relief. Comparison of figure 8 with figure 2 illustrates the effect of the greater range of smaller crater sizes in subduing the relief of the lunar surface features, which are softer than those on the simulated surface.

Although significant local variations exist (Trask, 1966, personal commun.; Shoemaker, 1965), crater-frequency distributions on the complex lunar surface are reasonably consistent with the predictions for a "steady-state" surface produced by repeated

impacts. It is difficult to account for such frequency distributions by processes other than repeated impacts. Erosion and infilling by repeated impacts readily explain the gradation from young craters with well-defined rims to old craters or shallow rimless depressions. In addition, erosion by impact and spallation can account for the fact that blocks range from angular to rounded in form. It should not be construed, however, that all the larger craters shown in the Ranger IX photographs are the result of impacts, for clearly they are not. Many are associated with rilles and are alined, and may thus be of internal origin (Kuiper and others, 1966; Carr, 1966).

Physical Properties of Lunar Surface

Comparison of the morphology of small lunar craters with that of experimental craters indicates that the upper lunar surface materials are fragmental and have very low cohesion, somewhat like that of moist sand. However, hard rock occurs below this layer of surface materials, as is indicated by the angular blocks in the ejecta blankets of many deep craters. The presence of an upper layer of weakly cohesive material was demonstrated for the area around Surveyor I by the impact of the 292 kg spacecraft with the lunar surface at about 3.6 m per sec (Jaffe and others, 1966). After nearly simultaneous impact of the three 30-cm diameter footpads, the lunar surface materials were pushed and ejected outward as the footpads moved outward and penetrated downward.

The presence of small smooth-rimmed craters around Surveyor I is consistent with the existence of a fragmental surface layer of low cohesion, and is also in agreement with the data from experimental cratering in moist sand. No evidence was found of deep rimless craters with depth-to-diameter ratios greater than 1, which are typical of experimental craters in blocks of pumice; nor was there evidence of small rimless craters with scattered blocks, which are typical of craters in indurated rocks. Since the small craters shown in Luna 9 panoramas and the smallest craters shown by Ranger IX have smooth raised rims around them, it is reasonable to conclude that in the areas photographed by both spacecraft the

surface is also underlain by very weakly cohesive fragmental materials. The absence of abundant blocks in the ejecta of the 13 to 25 m craters shown in the Ranger IX photographs tends to confirm the presence of the weakly cohesive layer.

The presence of a layer of hard rock beneath the surface materials around Surveyor I is revealed by the scattered blocks in ejecta from the 30 m diameter crater. The ejecta from this crater does not have the profusion of blocks expected from a homogeneous indurated material (see for example, fig. 6) but rather one from a layered material (see for example, fig. 5). Also, blocks in this ejecta are angular to rectangular, a characteristic common in indurated terrestrial rocks. Inspection of craters around Surveyor I that range from 3.4 to 6.3 m in diameter and have large blocks on their rim suggests that the blocks are from a layer about 1 m deep (Jaffe and others, 1966a). A few positive features which may be blocks excavated from a hard-rock layer occur around the larger craters shown by Ranger IX; however, these positive features could, instead, be mounds of debris.

In summary, current data on both experimental and lunar craters indicate that the lunar surface materials are layered. The uppermost layer is weakly cohesive and about 1 m deep near Surveyor I and possibly deeper in the area photographed by Ranger IX. This layer is at least 10 cm deep around Luna 9. A layer of indurated rock occurs beneath the soil-like layer of material in the vicinity of Surveyor I.

SUMMARY

Crater-frequency distribution shown in the high-resolution photographs taken by Ranger IX, Luna 9, and Surveyor I agrees well with the distribution that was calculated by combining data on impact cratering with data on the flux of meteoroids and other debris expected to impact the lunar surface, and with a crater-frequency distribution that resulted from a simulated meteoroid bombardment in the laboratory. Morphologically, fine-scale lunar craters,

craters predicted for a "steady-state," and craters produced during experiments after the "steady-state" was obtained all vary continuously from young unmodified craters to those so eroded and infilled that they are barely discernible. Thus, the fine-scale features of the lunar surface are consistent with the theory that the surface has been repeatedly cratered by impacts for a period sufficiently long to produce a "steady-state" in which the smaller craters are formed as rapidly as they are destroyed. Erosion by repeated impacts also offers a ready explanation for the variation in shapes of blocks and fragments on the lunar surface.

Young small craters considered to be the result of projectile impacts with the lunar surface are similar in morphology to terrestrial craters in materials with very low cohesion. The raised rims, smooth moderate slopes of the crater walls, circular outlines, and smooth ejecta blankets are common to both lunar craters and experimental craters in materials with very low cohesion, like that of moist sand.

Although the uppermost lunar materials are nearly cohesionless, large craters have some blocks in their ejecta which have been brought to the surface during crater formation by impact. The presence of blocks and fragments around craters about 6 m in diameter suggests that a hard-rock layer occurs about 1 m below the surface.

REFERENCES

Akademiya Nauk SSSR, 1966, The first panoramic views of the lunar surface: U.S. Natl. Aeronautics and Space Adm. Tech. Translation F-393, 125 p.

California Institute of Technology, Jet Propulsion Laboratory, 1966, Ranger IX photographs of the Moon: U.S. Natl. Aeronautics and Space Adm. Spec. Pub. 112, 17 p., 170 pls.

Carr, M. H., 1966, The structure and texture of the floor of Alphonsus, in Ranger VIII and IX, pt. 2, Experimenters' analyses and interpretations: California Inst. Technology, Jet Propulsion Lab. Tech. Rept. 32-800, p. 270-271.

Davis, W. M., 1909, Geographical essays: Boston, Mass., Ginn and Co., 777 p.

Fulmer, C. V., 1965, Cratering characteristics of wet and dry sand: Seattle, Wash., Boeing Co., Rept. D2-90683-1.

Fulmer, C. V., and Roberts, W. A., 1963, Rock induration and crater shape: Icarus, v. 2, no. 5/6, p. 452-465.

Gault, D. E., Quaide, W. L., and Oberbeck, V. R., 1966a, Interpreting Ranger photographs from impact cratering studies, in Conference on the nature of the lunar surface, Proceedings: Baltimore, Md., Johns Hopkins Press, p. 125-140.

Gault, D. E., Quaide, W. L., Oberbeck, V. R., and Moore H. J., 1966b, Luna 9 photographs--Evidence for a fragmental surface layer: Science, v. 153, no. 3739, p. 985-988.

Jaffe, L. D., 1965, Depth of the lunar dust: Jour. Geophys. Research, v. 70, no. 24, p. 6129-6138.

Jaffe, L. D., and others, 1966a, Surveyor I mission report, pt. 2, Scientific data and results: California Inst. Technology, Jet Propulsion Lab. Tech. Rept. 32-1023, 100 p.

_____1966b, Surveyor I--Preliminary results: Science, v. 152, no. 3730, p. 1737-1750.

Kuiper, G. P., Strom, R. G., and LePoole, R. S., 1966, Interpretation of the Ranger records, in Ranger VIII and IX, pt. 2, Experimenters' analyses and interpretations: California Inst. Technology, Jet Propulsion Lab. Tech. Rept. 32-800, p. 35-248.

Moore, H. J., 1964, Density of small craters on the lunar surface, in Astrogeologic Studies Ann. Prog. Rept., August 25, 1962 to July 1, 1963, pt. D: U.S. Geol. Survey open-file report, p. 34-51.

_____1966, Cohesion of material on the lunar surface, in Ranger VIII and IX, pt. 2, Experimenters' analyses and interpretation: California Inst. Technology, Jet Propulsion Lab. Tech. Rept. 32-800, p. 263-270.

Moore, H. J., Gault, D. E., Heitowit, E. D., and Lugn, R. V., 1964a, Hypervelocity impact craters in porous cohesive targets, in Astrogeologic Studies Ann. Prog. Rept., July 1, 1963 and July 1, 1964, pt. B: U.S. Geol. Survey open-file rept., p. 93-143.

Moore, H. J., Kachadoorian, Reuben, and Wilshire, H. G., 1964b, A preliminary study of craters produced by missile impact, in Astrogeologic Studies Ann. Prog. Rept., July 1, 1963 to July 1, 1964, pt. B: U.S. Geol. Survey open-file rept., p. 58-92.

Murphy, B. F., 1961, High-explosive crater studies--Desert alluvium: Sandia Corp. Rept. SC-4614, 44 p. (Prepared for U.S. Atomic Energy Comm.)

Polatty, J. M., and Curry, R. L., 1964, Investigation of the feasibility of manufacturing aggregate by nuclear methods: Vicksburg, Miss., U.S. Waterways Expt. Sta., 19 p., 1 table, 15 photos.

Shoemaker, E. M., 1960, Penetration mechanics of high velocity meteorites, illustrated by Meteor Crater, Arizona: Internat. Geol. Cong., 21st, Copenhagen 1960, Rept., pt. 18, p. 418-434.

_____1965, Preliminary analysis of the fine structure of the lunar surface of Mare Cognitum, in Ranger VII, pt. 2, Experimenters' analyses and interpretations: California Inst. Technology, Jet Propulsion Lab. Tech. Rept. 32-700, p. 75-134.

Trask, N. J., 1966, Size and spatial distribution of craters estimated from the Ranger photographs, in Ranger VIII and IX, pt. 2, Experimenters' analyses and interpretations: California Inst. Technology, Jet Propulsion Lab. Tech. Rept. 32-800, p. 252-263.

Vortman, L. J., 1966, Craters from shory-row charges and thin interaction with pre-existing craters: Sandia Corp. Rept. SC-RR-66-324.

Vortman, L. J., Chabai, A. J., Perret, W. R., and Reed, J. W., 1962, Buckboard, final report: Sandia Corp. Rept. SC-4675, 308 p. (Prepared for U.S. Atomic Energy Comm.)

Whipple, F. L., 1963, On meteoroids and penetration: Jour. Geophys. Research, v. 68, no. 17, p. 4929-4939.

SITE REPORTS MADE IN PREPARATION FOR THE LUNAR ORBITER I MISSION

Nine reports were prepared on the geology of the primary sites to be photographed by the first Lunar Orbiter mission in order to provide a geologic base of information prior to the flight. These reports summarized the terrestrially derived geologic, topographic photographic, infrared, and albedo data that were then available. Interpretations based on these data were presented in a format approximating that of the reports anticipated for the Lunar Orbiter mission. The reports were available during the screening session and were very useful in plotting the photographs, identifying features, interpreting geology and terrain at the larger scales, and, generally, in bridging the gap between terrestrial observation and the first orbital photography of the Moon.

The reports also enabled comparison of geologic interpretations based on terrestrial observation with those based on orbital photographic observations. This comparison clearly indicated that orbital photography is of enormous benefit in recording details of lunar surface features, but that the stratigraphic basis derived from terrestrial observations is sound. No sweeping revisions of the stratigraphic basis of regional lunar geology are foreseen.

One of the pre-Lunar Orbiter site reports is presented here. It covers an area for which the amount and quality of terrestrially derived information were about average. Reports on the other eight sites appeared as Technical Letters Astrogeology 14 through 21.

PRE-FLIGHT EVALUATION OF LUNAR ORBITER SITE A-1

By Terry W. Offield

INTRODUCTION

The center of site A-1 is at lat 0°50' S. and long 42°20' E. The area evaluated is a rectangle, about 40 × 120 km, slightly larger than the projected Orbiter photograph coverage at 8-meter resolution. This rectangle is inclined 12°00' clockwise with respect to the lunar equator.

Information from available geologic and terrain maps (Elston, 1965; Holm, Rowan, and McCauley, 1966) has been somewhat updated for this report by telescopic observation and study of recent good-quality photographs. The best photographs of the site are Catalina 731 and 696 and Lowell L7-193-6-1; Catalina 103, 223, and 226 offer better resolution of a few specific features. The photographic resolution is about 1 km or slightly better.

GEOLOGY

Regional Setting

Site A-1 lies half in Mare Fecunditatis and half in the uplands that separate it from Mare Tranquillitatis (fig. 1).

Crater Secchi X is the most prominent feature in the mare part of the site. At slightly better than 1-km resolution, about 40 percent of the mare area around Secchi X is virtually featureless. The remainder is characterized by low ridges, principally the subdued rim of a large crater older than the mare filling. Two large low domes, one of which seems to have a summit crater, occur within this old crater, and the west rim of the crater is cut by a rille connecting two small domes.

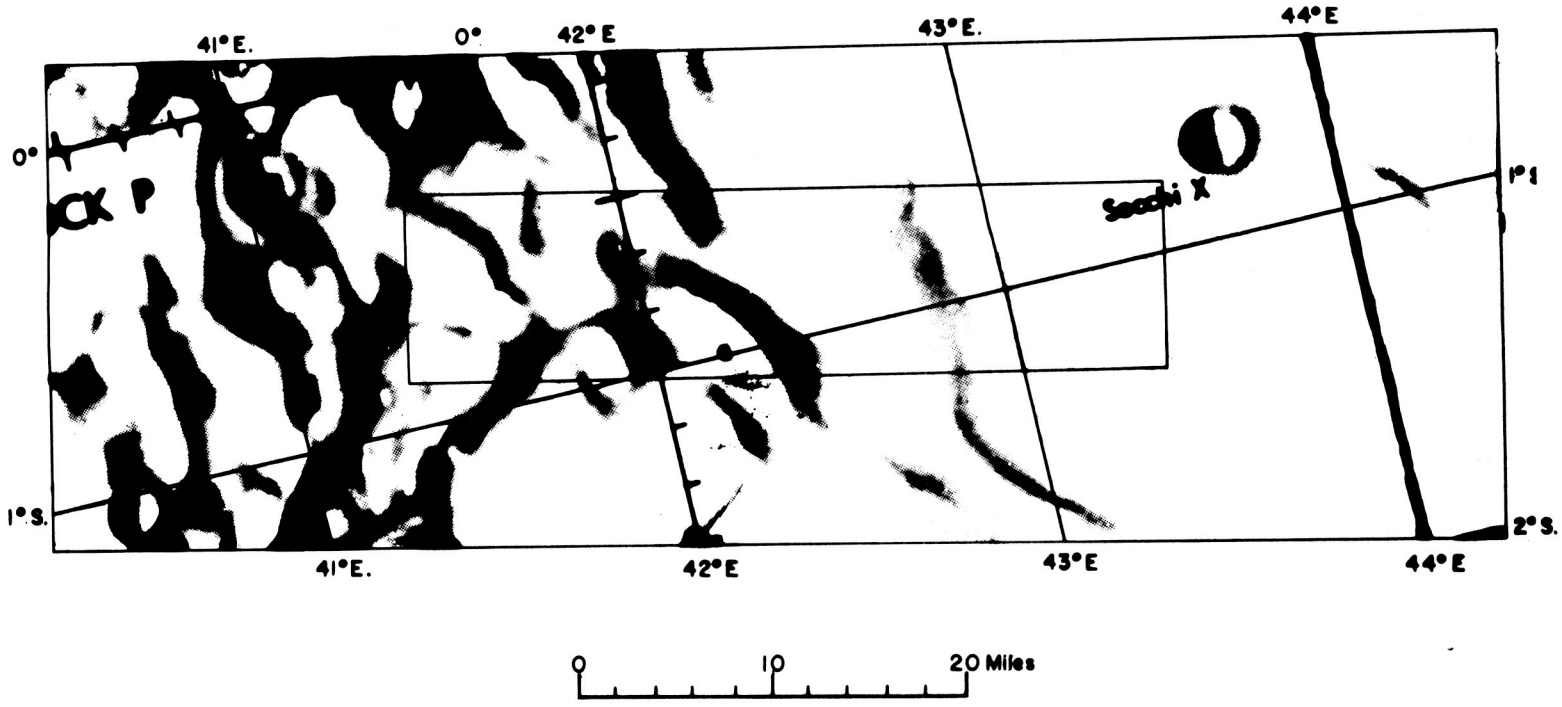

Figure 1.--Outlines of high-(small rectangle) and low-(large rectangle)resolution photographic coverage. Base source ACIC LAC 61 and 79.

A straight rille about half a mile wide crosses the northeast corner of the site.

The upland area is 300-600 meters above the general mare level and its maximum relative relief is about 300 meters (ACIC LAC 79, contour data). The mare-uplands contact is generally sharp but varies in character from a steep scarp to a change from smooth mare to relatively low-lying hummocky upland materials. The uplands front is broken at the center of the site, and the indentation is filled by a low dome that has a summit crater connected by a small rille to at least two other craters.

The northwest edge of the site extends into the crater Lubbock P, which opens northwestward into Mare Tranquillitatis; the floor of the crater is the darkest area in the site. The moderately steep east wall of Lubbock P appears to have been modified by faults and slumping.

General Stratigraphy

The oldest geologic units are the pre-Imbrian Censorinus and Secchi Formations of the uplands (fig. 2), both interpreted by Elston (1965) to be ejecta deposited during the excavation of mare basins to the north and east. The Censorinus Formation is characterized by broadly undulating surfaces, steep slopes at places, and relatively high albedo. Old craters in the Censorinus Formation are greatly modified in form. The Secchi Formation is younger than the Censorinus Formation, is undulatory on a smaller scale (2 km), and has a lower albedo. It may be partly volcanic in origin.

Units of uncertain age (pre-Imbrian-Eratosthenian?) that are probably volcanic have been split from Elston's (1965) Secchi Formation on the basis of new information. One such unit is the cratered dome at the embayment in the uplands front, which strongly resembles a shield volcano; its material merges eastward with the mare material without a noticeable break. Another probable volcanic unit is the slightly hummocky to smooth upland-plains-forming unit designated IpIs in figure 2. In the uplands just

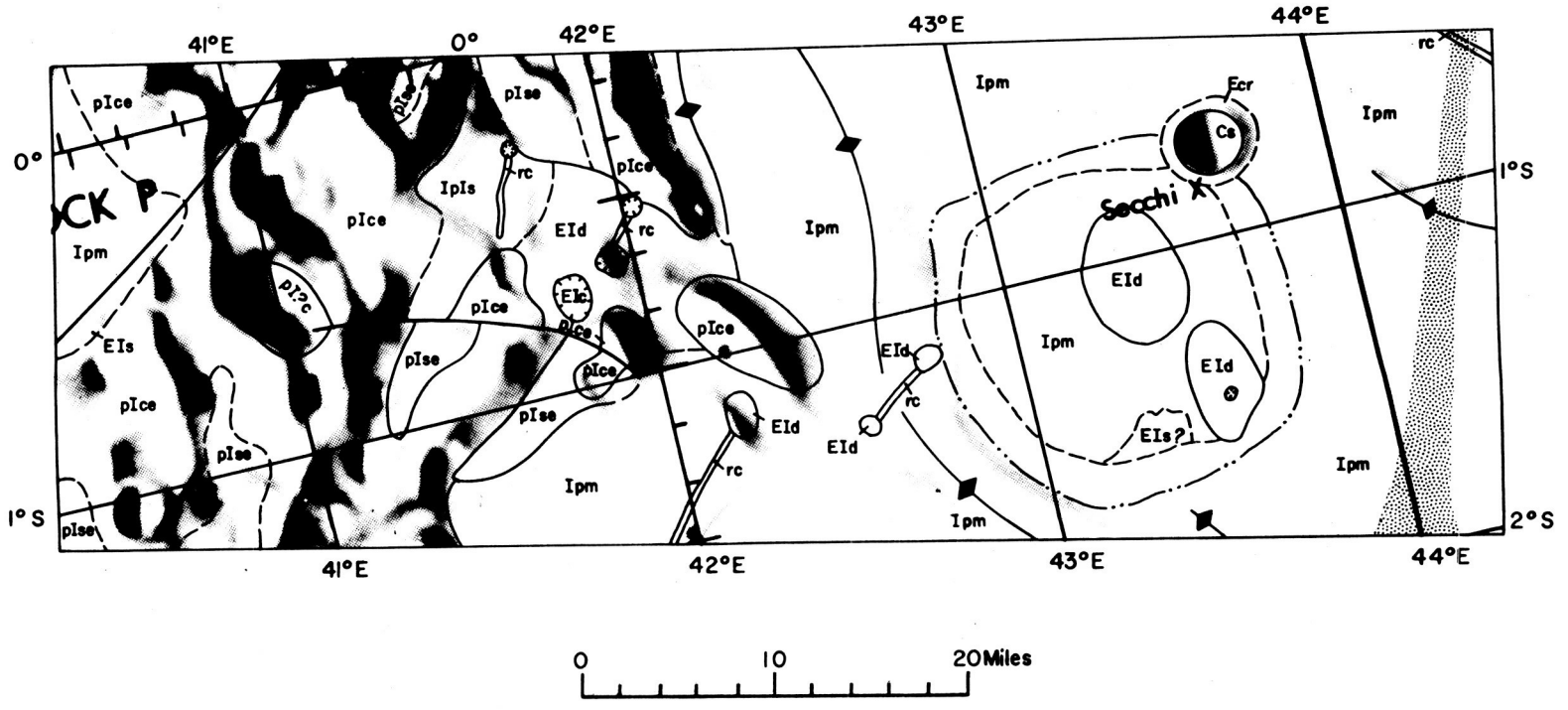

Figure 2.--Geology and relief. Base source ACIC LAC 61 and 79.

EIs

Slump material

Characteristics
Material of irregular outline and variable low to intermediate albedo at base of crater inner walls.

EId

Dome material

Characteristics
Domes are broad and low to small and pluglike in form. Some have summit craters, some appear to be lighter in color than surrounding mare material. Pluglike domes associated with rilles.

Interpretation
Probably shield volcanoes and volcanic plug domes.

EIc

Crater material

Characteristics
Crater is rimless and shallow.

Interpretation
Possibly collapse feature or shallow vent on flank of volcano.

Cs

Slope material

Characteristics
Occurs on inner wall of Secchi X; Albedo very high.

Interpretation
Bedrock (?) and fragmental material freshly exposed by slumping on crater wall.

COPERNICAN SYSTEM

Ecr

Crater rim materials

Characteristics
Intermediate albedo.

ERATOSTHENIAN SYSTEM

Ipm

Mare materials

Characteristics
Albedo low where unit not covered by ray scatter; relatively smooth surface broken by rilles and broad low ridges and domes.

Interpretation
Volcanic materials; flows and (or) ash beds.

IMBRIAN SYSTEM

IpIs

Smooth upland material

Characteristics
Smooth to slightly hummocky surfaces of low-intermediate to intermediate albedo in low areas of uplands.

Interpretation
Materials, either volcanic or fine ejecta, blanketing and variably subduing irregular older surfaces.

PRE-IMBRIAN OR IMBRIAN SYSTEM

pIc

Crater material

Characteristics
Crater form modified by faulting.

pIse

Secchi Formation (Elston, 1965)

Characteristics
Coarsely hummocky surfaces of low-intermediate to intermediate albedo in low areas of uplands.

Interpretation
Interpreted by Elston as mare-basin ejecta; may be blanketed to various degrees by smooth upland material.

pIce

Censorinus Formation (Elston, 1965)

Characteristics
Broadly undulating upland surface with fine-scale irregularities; albedo intermediate to high intermediate. Contains rimless craters.

Interpretation
Fragmental materials, perhaps one or more deposits of ejecta from mare basins.

PRE-IMBRIAN

Contact
Dashed where approximately located.

Fault

Mare Ridge
Line marks crest.

Buried crater rim

rc
Rille and chain crater

Well-developed ray pattern

south of the site at least two other distinctive probably volcanic blanketing units can be defined; one of these is noticeably dark.

The mare filling is considered to be volcanic material of Imbrian age that covers but does not completely subdue the rim of a large older crater. Domes with and without visible summit craters occur on the mare surfaces; these are designated EId in figure 2 and are easily seen in figure 3. The large domes may be volcanoes or expressions of subsurface intrusions. The smaller, sharper domes may be volcanic plug domes. The domes are of unknown post-mare age, but may be related in time to the probable volcanic units of the uplands. Mare ridges are probably expressions of subsurface intrusions. Crater Secchi X is relatively sharp rimmed but rayless. It is considered to be Eratosthenian, with bright inner slopes formed by mass wasting during Copernican time.

On the best full-moon photographs, most of the mare area of the site is weakly to moderately bright owing to variable but ubiquitous "ray" scatter (fig. 4). The eastern edge of the site is within a well-defined ray of Taruntius. Just south of the site is a very straight ray of Messier A. Two small areas of fairly dark mare occur in the southeast part of the site near the junction of the Taruntius and Messier rays.

Figure 4 clearly shows the variation in albedo in the uplands, which is helpful in defining stratigraphic units. The variation in albedo in the mare is related to "ray" scatter and, therefore, probably to variation in crater frequency. Four fairly distinct brightness subunits, ranging from dark mare to strongly developed ray, may be defined in the mare portion of the site. The albedo variations described are not very evident in the contoured relative albedo units of figure 5, which, instead, very closely reflect topography. The relative albedo units range from 5 to 25. In other sites the darkest relative unit is -1 and the brightest 35.

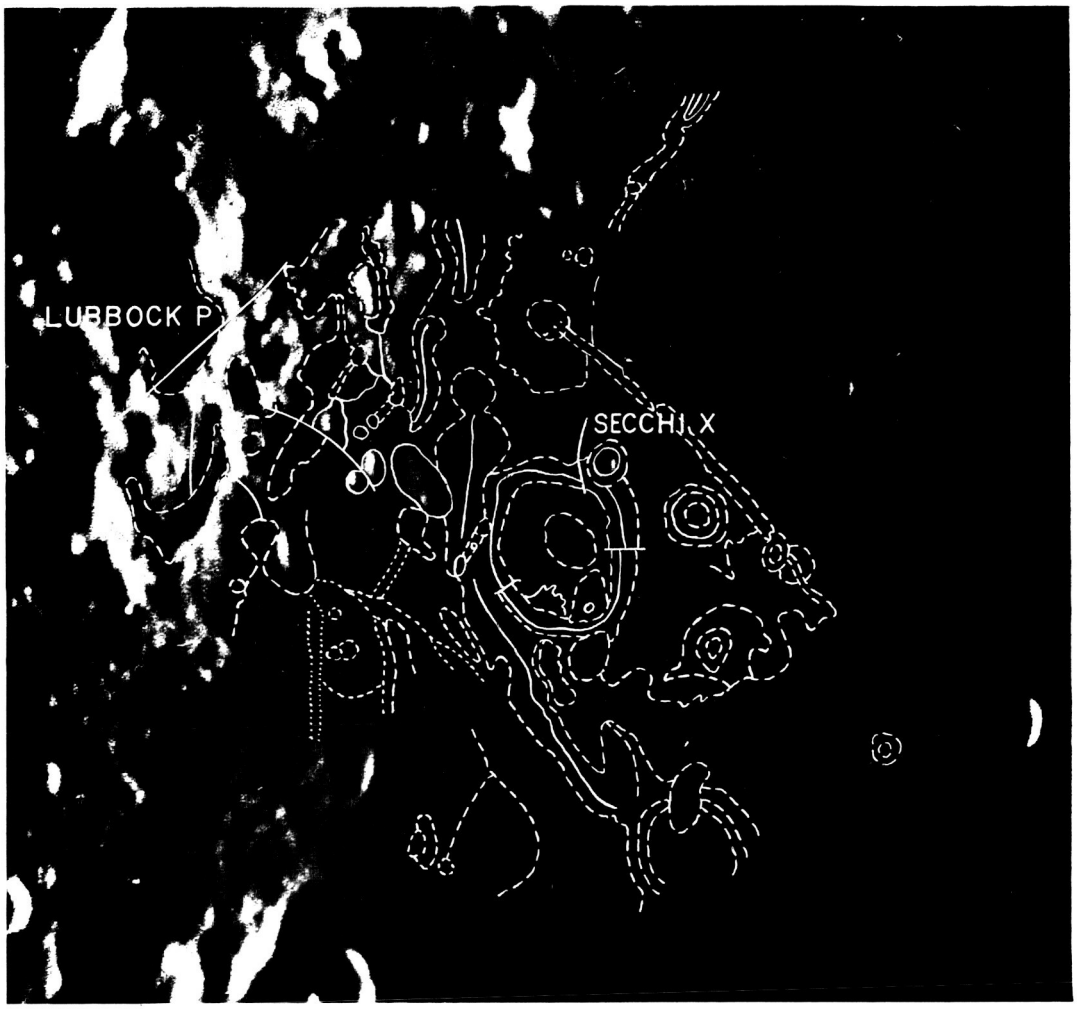

Figure 3.--Geologic and topographic detail partly annotated on unrectified photograph. Units compare with figure 2. Photograph by Catalina Observatory.

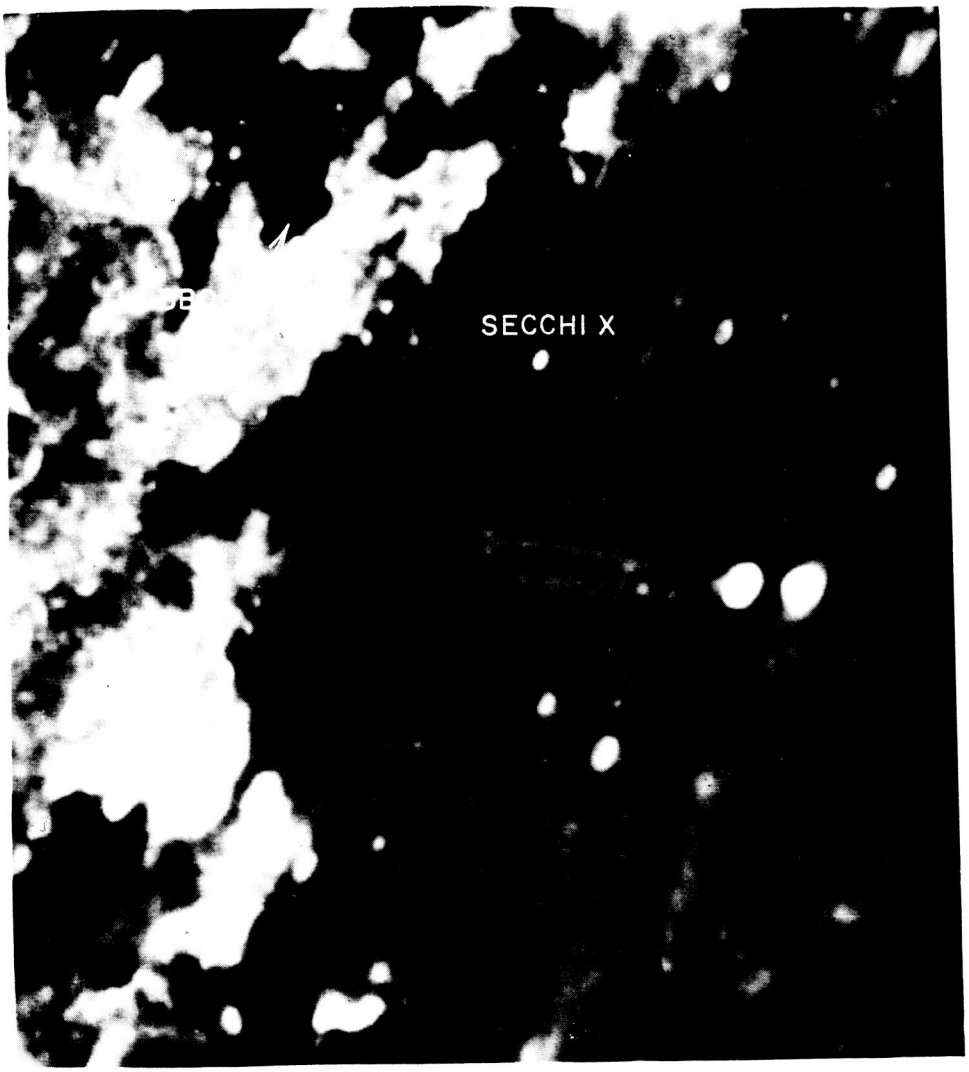

Figure 4.--Full-moon photograph of site A-1; note ray scatter in mare and albedo variation in uplands.

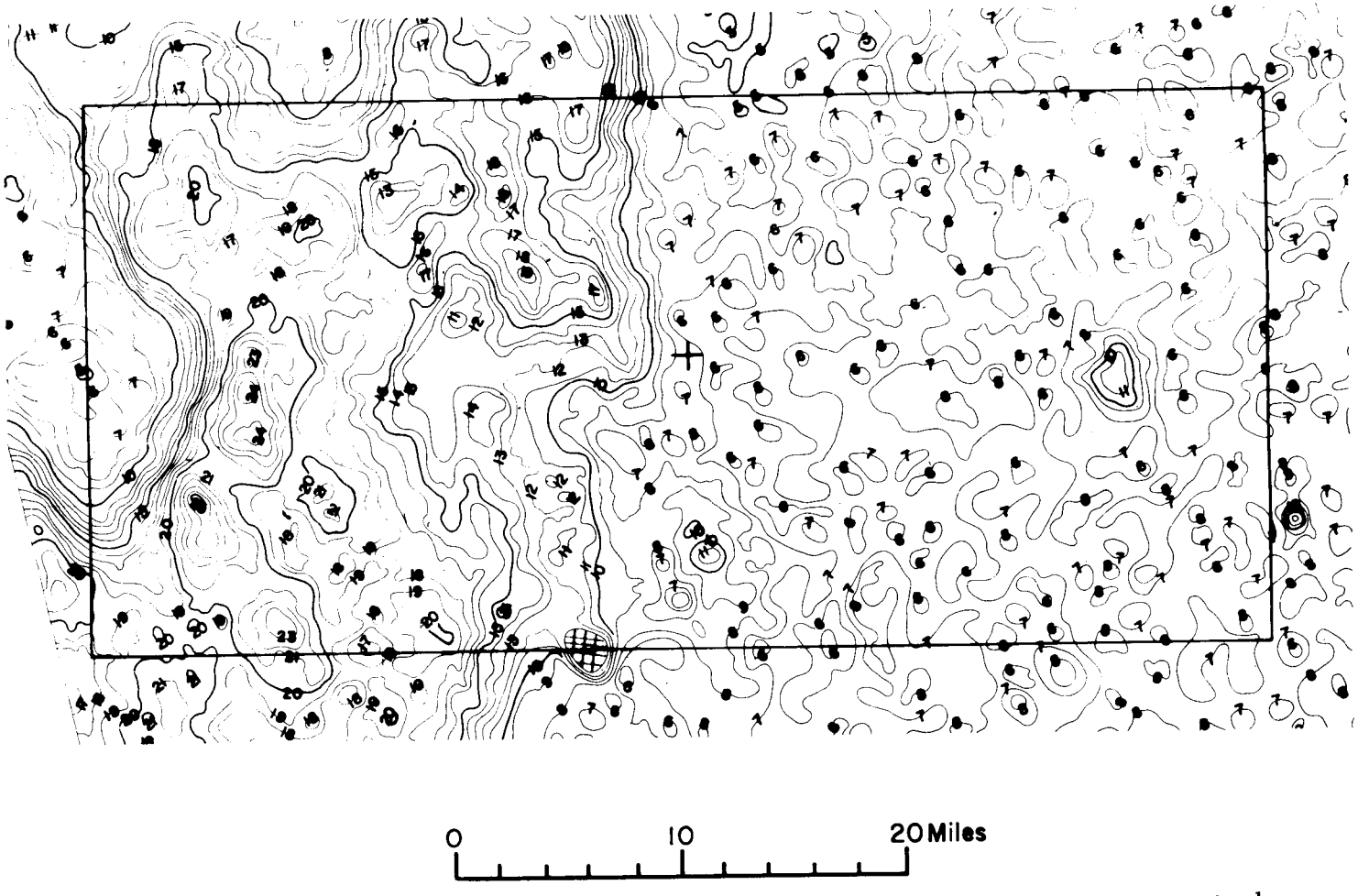

Figure 5.--Relative normal albedo. Crosshatch indicates increase in density too great to be measured. Coordinates of center of rectangle are lat 0°50' S., long 42°20' E; g (phase angle) = 1°55'12". Because area is on lunar limb, east-west directions are foreshortened and bar scale applies only to distance measured north-south.

Infrared measurements reported by Saari and Shorthill (1966) show that crater Secchi X is a strong positive thermal anomaly and crater Lubbock P is thermally negative relative to the adjacent uplands and mare.

Structural Geology

Linear features (fig. 2) include faults, rilles, chain craters, and irregular troughs. Lubbock P and a smaller crater nearby in the uplands are cut and somwhat modified in outline by prominent faults. Rilles in both uplands and mare connect craters or domes and appear to terminate in chain craters. The linear features trend north, northeast, and northwest matching well-known global lineament systems.

Terrain Analysis

Figure 6 shows the detailed subdivision of terrain units in site A-1. Three types of terrain in the mare area were defined for statistical comparison (fig. 7): smooth mare; low ridges, including the rim of the large crater and the area within the crater; crater Secchi X; a relatively sharp single ridge parallel to the mare-uplands contact. Figure 8 and table 1 show that (excluding Secchi X) the mare terrain units are similar. Slopes of more than 2° are uncommon and occur only in the ridges and the old crater-rim area. The standard deviation of 0.88 for the total mare area falls in the terrain category of smooth mare (fig. 9).

Useful statistical data for terrain subareas (fig. 7) in the uplands of site A-1 are not available. The subareas, however, were defined from study of good photographs, and morphologic comparisons can be made. Subarea 5 is probably a shield volcano bisected by a line of craters. The slopes of this domical feature are gentle and appear to be fairly smooth. Subarea 6 is a plain, smooth to slightly hummocky, broken in one place by a rille. It is lower than the surrounding uplands and higher than the adjacent flank of the probable volcano. Subarea 7 is the largest and most diverse uplands terrain sample. It includes ridges and linear

troughs, modified old craters, and broadly undulating plateaus, and is evidently structurally complex. Subarea 8 is arcuate, hummocky, cratered, and lower than the surrounding terrain. Subarea 9 is the smooth, dark, mare-covered floor of Lubbock P crater. Apparently it is crossed by a fault and covered with slump materials at the eastern edge. No craters with Eratosthenian or Copernican characteristics are visible in the uplands.

The mare of subarea 1 and large parts of subarea 2 (fig. 7) at 1-km resolution appears suitable for Apollo landings. However, the diffuse brightness of the mare is probably due to a high density of small craters in most of the area. If so, the surface may be badly churned up, and therefore rougher and possibly less firm than the relatively darker mare on which Surveyor I landed. The plains and somewhat rounded plateau areas in the uplands offer possible emergency landing sites.

Table 1.--Slope statistics for mare area

Subarea	Number	σ_{AL}	Slope reversal (percent)	10-90 percent	$\bar{x}_{Ab}$
1	234	0.69	15	1.00	0.54
2	374	.86	16	1.35	.72
3	---	---	---	---	---
4	33	.69	24	1.55	.67
All mare	*775	.88	17	1.75	.69

*Includes subarea 3, and very small area of adjacent uplands.

SUMMARY

Site A-1 lies half in mare and half in uplands. Features of the mare part include smooth mare, ridges, buried or subdued old crater rims, domes, an Eratosthenian crater, rilles, and variation from dark mare to strong ray areas. Upland features include plateaus, ridges and troughs, smooth to hummocky plains, a probable shield volcano, chain craters and rilles, and modified old craters. The mare-uplands contact is variable, probably both structural and

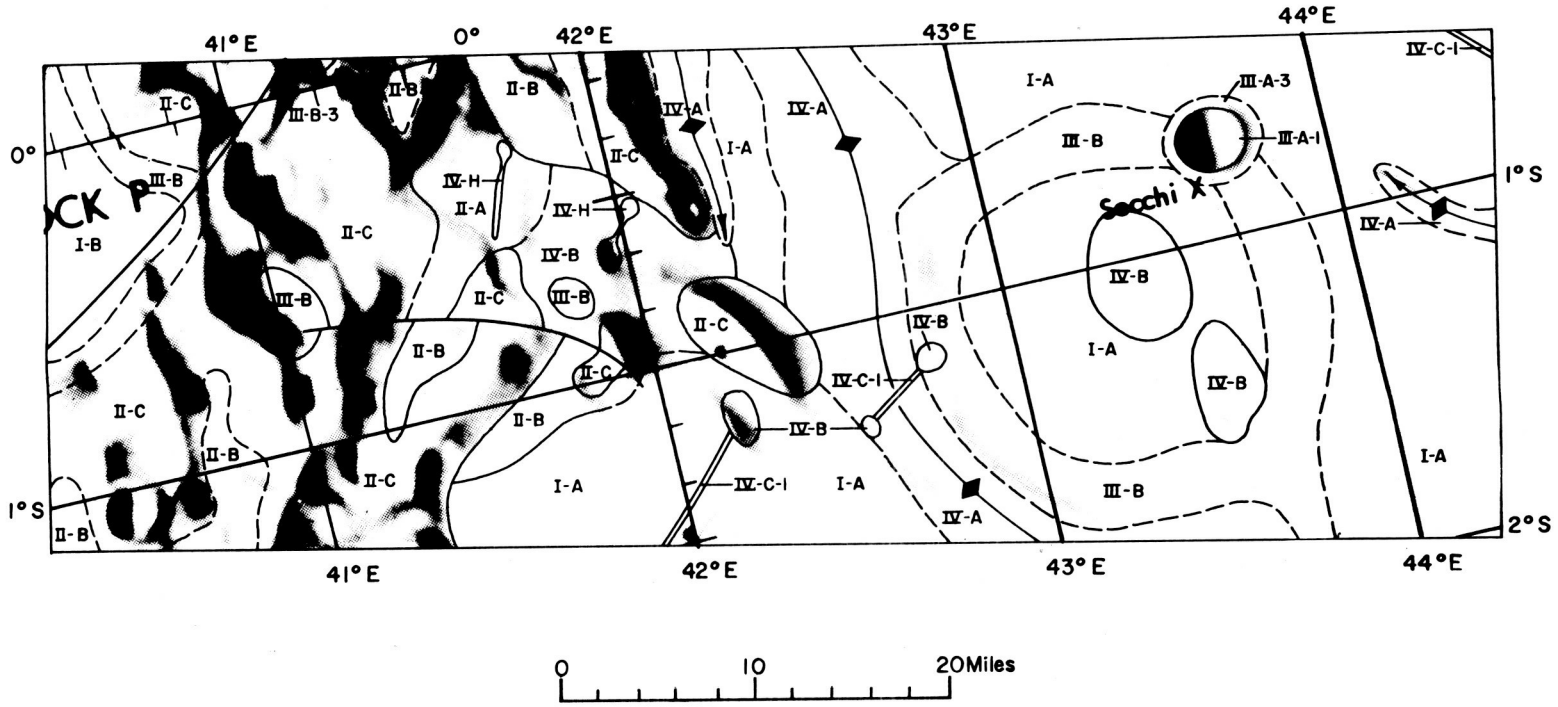

Figure 6.--Terrain units. Base source ACIC LAC 61 and 79.

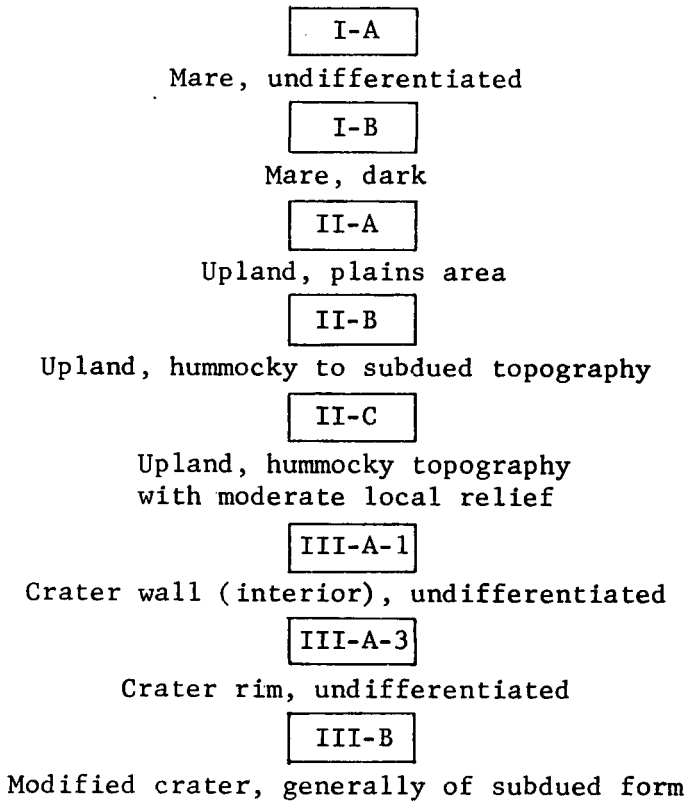
I-A
Mare, undifferentiated
I-B
Mare, dark
II-A
Upland, plains area
II-B
Upland, hummocky to subdued topography
II-C
Upland, hummocky topography with moderate local relief
III-A-1
Crater wall (interior), undifferentiated
III-A-3
Crater rim, undifferentiated
III-B
Modified crater, generally of subdued form
III-B-3
Crater rim; subdued, hummocky topography
IV-A
Ridges, located within mare
IV-B
Domes
IV-C-1
Rilles
IV-H
Chain craters
Definite boundary
Indefinite boundary
Ridge crests
Faults

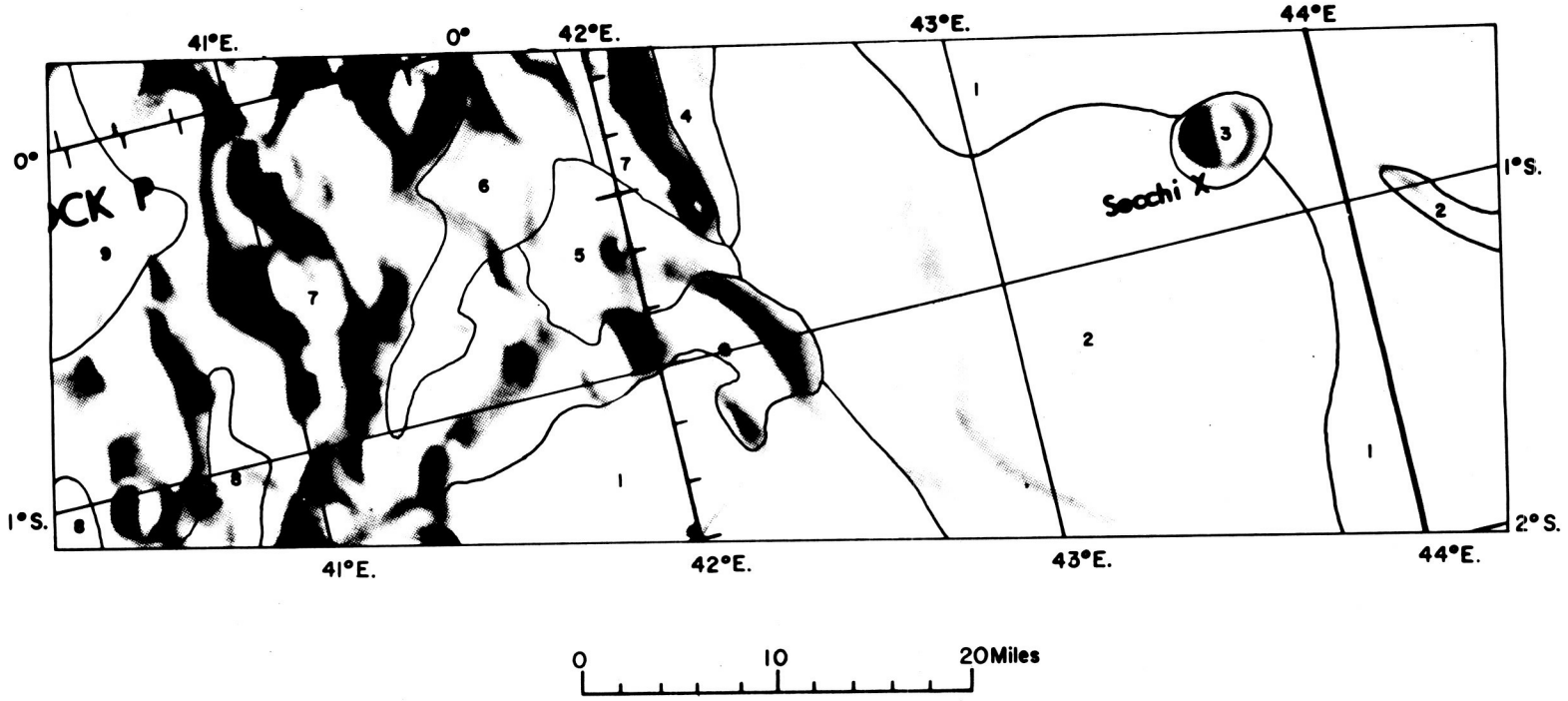

Figure 7.--Slope-statistics subareas. Base source ACIC LAC 61 and 79.

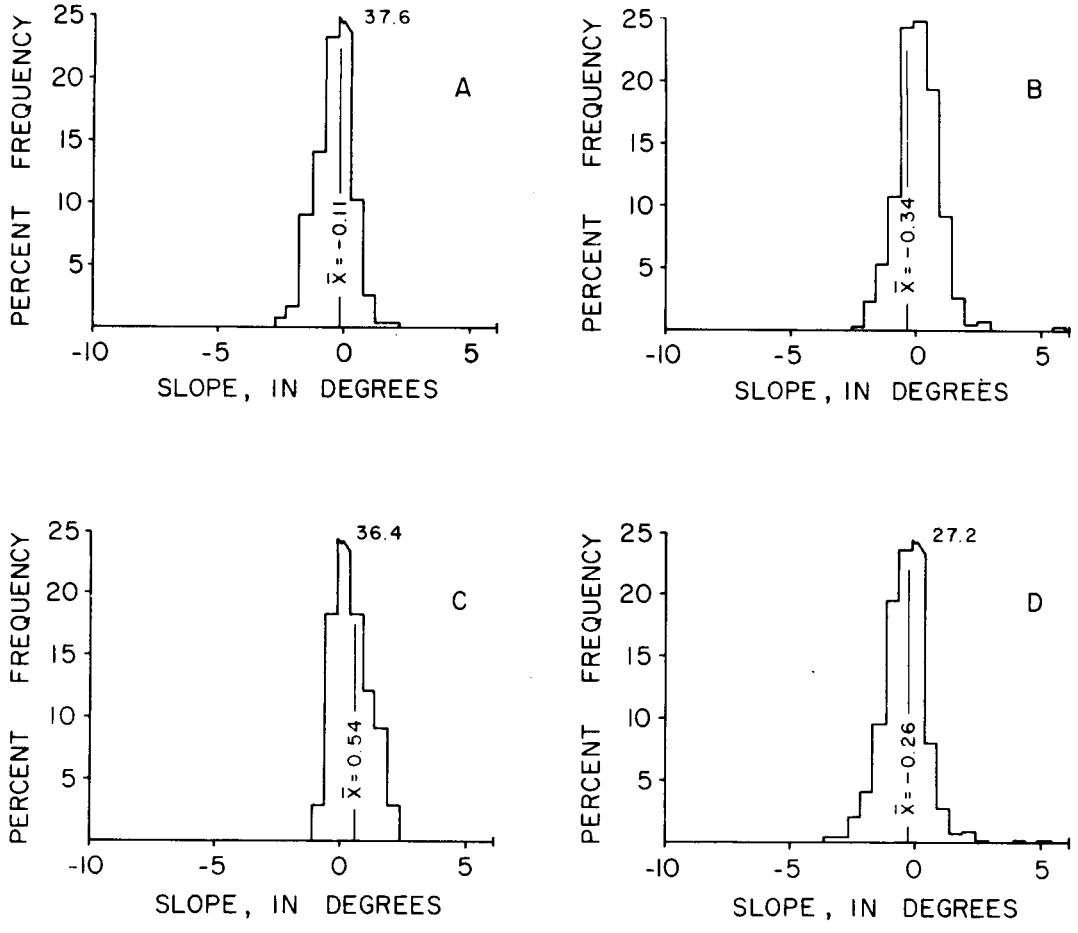

Figure 8.--Histograms showing algebraic slope-frequency distribution. A, subarea 1; B, subarea 2; C, subarea 4; D, total mare.

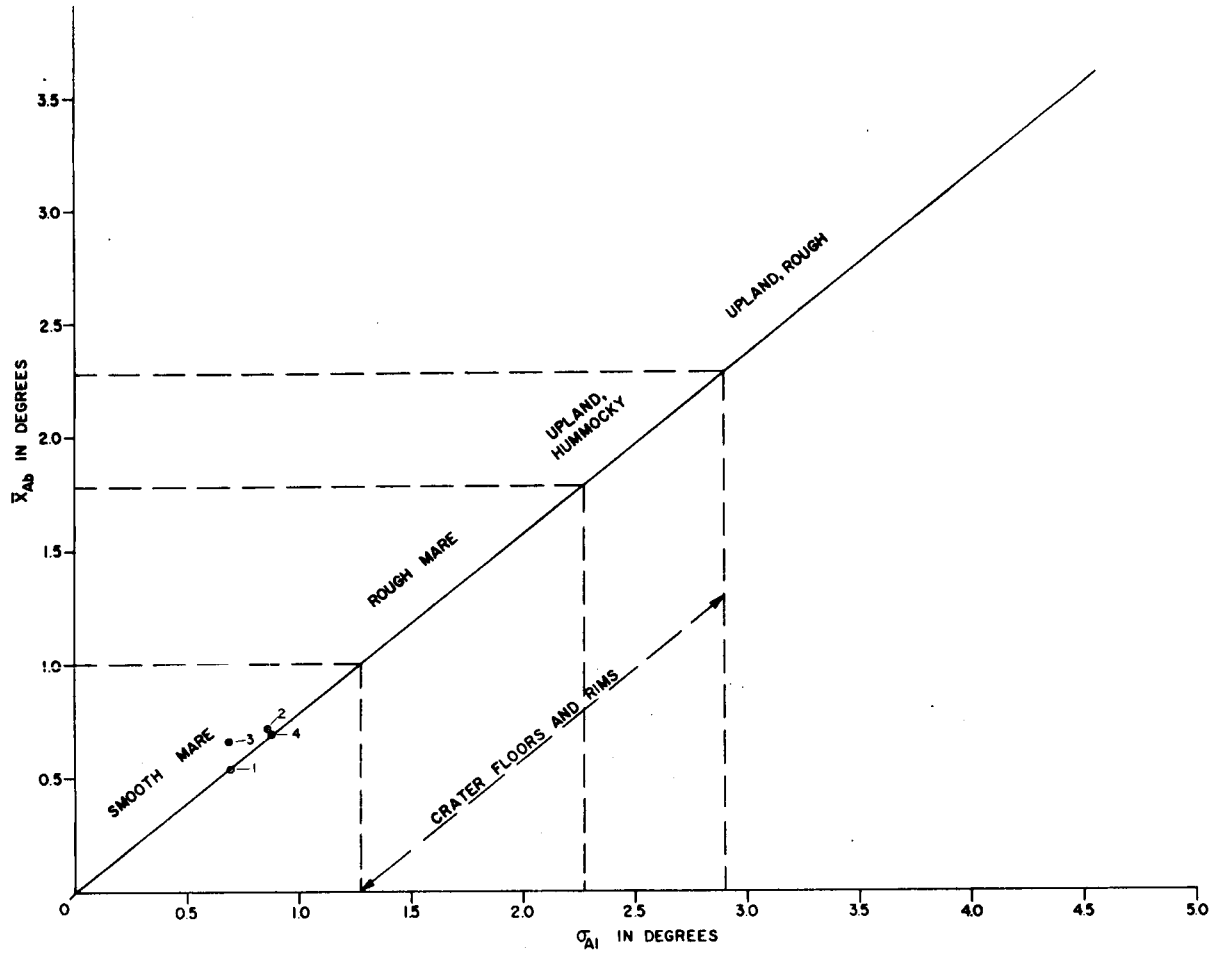

Figure 9.--Lunar roughness scale (algebraic standard deviation versus absolute arithmetic mean).

depositional in nature, and will be very interesting to study at Orbiter photographic resolution. Albedo variations are conspicuous in both mare and uplands, and Orbiter photographs should enable linking these variations to differences in uplands geologic units and to surface characteristics in the mare.

For Apollo landings, the smooth mare areas are the best possibility. Alternate landing areas could include ridge areas in the mare and the plains and plateaus of the uplands.

Features of considerable geologic interest which will be prominent in the Orbiter pictures are as follows:

1. Rille in northeast corner of site, especially if coverage includes crater chain at southeast end of sharp rille.
2. Subdued rim of large old crater in mare (the one with Secchi X on its northeast corner) and domes within the crater.
3. Mare ridge and adjacent mare-uplands contact.
4. Dome (cone?) with summit crater(s) and rille (chain crater?) leading northeastward from summit. Slightly west and north of center of site.
5. Positive feature with possible lobe extending east and rille extending south-southwest from it. South of uplands promontory in center of site.
6. Division of uplands: Dominant smooth bright uplands, in part with linear troughs; hummocky darker unit (southwest corner of site); smooth to slightly hummocky plains-forming unit, cut by rille (northwest of dome with summit crater; at north edge in west half of site).
7. Lubbock P crater; dark floor except southeast of lineament which cuts across southeast corner of crater.
8. Lineaments in uplands.
9. Character of diffusely bright (scattered ray?) areas in mare.

REFERENCES

Elston, D. P., 1965, Preliminary geologic map of Colombo quadrangle, in Astrogeologic Studies Ann. Prog. Rept., July 1964-July 1965, map supp.: U.S. Geol. Survey open-file rept.

Holm, E. A., Rowan, L. C., and McCauley, J. F., 1966, Preliminary terrain map of the lunar equatorial belt: U.S. Geol. Survey, unpub. map.

Saari, J. M., and Shorthill, R. W., 1966, Isotherms in the equatorial region of the totally eclipsed moon: Boeing Sci. Research Lab., Geo-astrophysics Lab., Doc. DI-82-0530.